PHYSICAL REVIEW B VOLUME 46, NUMBER 10 1 SEPTEMBER 1992-II

General multiple-scattering scheme for the computation and interpretation of x-ray-absorption fine structure in atomic clusters with applications to SF_6, $GeCl_4$, and Br_2 molecules

T. A. Tyson and K. O. Hodgson
Department of Chemistry, Stanford University, Stanford, California 94305

C. R. Natoli and M. Benfatto
Laboratori Nazionali di Frascati dell'Istituto Nazionale di Fisica Nucleare, P.O. Box 13, 00044 Frascati, Italy

(Received 5 August 1991; revised manuscript received 24 March 1992)

We present a general multiple-scattering (MS) scheme utilizing complex potentials for the calculation and interpretation of inner-shell x-ray-absorption fine structure for clusters of atoms in condensed matter with application to the case of the molecules SF_6, $GeCl_4$, and Br_2. The method is based on the solution of the Dyson equation with a complex self-energy of the Hedin-Lundqvist type for the single-particle Green's function describing the propagation of the excited photoelectron through the system. We also address the problem of the equivalence between two traditional approaches to this kind of calculation: the scattering approach of Dehmer and Dill and the density-of-states (or MS) approach of Lee and Pendry. The application of the theory to the calculation of the extended fine structure in the three molecules shows that one can get amplitude agreement without introducing intrinsic loss reduction effects, which seem therefore to be negligible. Some minor problems with absolute phase agreement still remain in some cases.

I. INTRODUCTION

Since the papers of Johnson[1] for bound states and Dill and Dehmer[2] for continuum states, multiple-scattering (MS) theory has been used as an interpretative tool for understanding electronic structure of a large variety of molecular systems because of the ease with which calculations can be carried out (even for large molecules). In the practical application to actual calculations, the MS method employs two important approximations: (a) the $X\alpha$ or statistical exchange approximation and (b) the muffin-tin (MT) averaging of the potential needed for the MS expansion of the wave functions. In this latter approximation the potential is spherically averaged in the atomic and outer-sphere regions and volume averaged in the interatomic (interstitial) region. The use of a constant interstitial potential is certainly a serious approximation and makes the results depend on the size of the interstitial region itself. There is now enough evidence, drawn from a variety of applications, that a "judicious" choice of MT radii, tailored to the physical properties of the system under study, does lead to physically acceptable results for bound states and continuum calculations in x-ray-absorption spectra (XAS).[3]

As shown in Ref. 4, the restrictions imposed by the MT approximation can be lifted through a formulation of the MS theory that takes into account both the nonspherical nature of the potential inside the atomic spheres and the fact that the potential is not constant in the interstitial region. In this approach the structure of the theory itself is unchanged, only the definitions of the atomic T matrices and spherical wave propagators (see Refs. 1 and 4) are changed. This formulation has been implemented in a computer code and work is in progress to assess the effects of the departure of the potential from its approximate MT form both for bound and continuum states.[5] Since we conceive this paper as being methodological in character with regard to the application of MS theory to the study of electronic and structural properties of molecular systems, we retain here the MT approximation. This choice will make the discussion simpler, while keeping all essential features of the MS approach. Preliminary calculations performed in a MS non-MT scheme for the SF_6 molecule have substantially confirmed the results obtained here within a MT scheme.

The $X\alpha$ approximation to the exchange correlation (EC) potential can be easily eliminated (both for bound and continuum calculations). For the continuum region we use, in fact, the now well-tested Hedin-Lundquist (HL)[6] energy-dependent EC potential. We only need to recalculate for each energy point the exchange-correlation part of the potential, using the local density $\rho(\vec{r})$ of the molecular system, and add it to the energy-independent Coulomb potential to obtain the total potential [see Ref. 6(a) for a comprehensive account of this potential and Ref. 7 for a short summary of the real part]. For bound-state calculations of the final state instead we use the more familiar $X\alpha$ approximation.

The procedure followed in Ref. 8 for the study of K edges of transition metal complexes was repeated in order to calculate the bound-state contribution as well as the continuum part of the spectra (up to 700 eV above threshold) for SF_6, $GeCl_4$, and Br_2 molecules, as representative of the most usual coordination geometries. The difference here is that we now use the T matrix or propagating wave normalization instead of the more standard

K matrix or standing wave normalization, as used in Refs. 2 and 8. The advantage is twofold. One can use the same concepts to describe not only the continuum part but also the bound-state part of the spectrum, when bound states, usually lying above the muffin-tin (MT) interstitial level, are available for transition. This description, known as the extended continuum (MS-EC) approach[9] treats the bound states as very narrow scattering resonances ultimately leaking away from the molecular region in a continuum state instead of decaying exponentially as true bound states do. Since the resonances are very narrow, their positions are little or not at all affected by the change in boundary conditions so that in this way the same single continuum calculation gives the energy separation between the bound-state features and continuum features (as, for example, shape resonances). However, the transition amplitude in the bound-state region might be incorrect, due to the different normalization procedures used for bound and continuum states, but this can be remedied by performing actual bound-to-bound transition amplitude calculations. In the case of free molecules this approach eliminates the need for positioning the bound-state features with respect to the ionization threshold and actually is close to reality for molecules in solution.

The second advantage is even more rewarding. By using a T-matrix normalization for the entire cluster and a suitable normalization for the radial solutions of the Schrödinger equation (SE) inside the various MT spheres, one can relate the wave-function amplitude inside the photoabsorber's atomic sphere to the scattering amplitude via a generalized optical theorem.[4(a)] Therefore it becomes possible to connect the square of the wave-function amplitude, which is proportional to the absorption coefficient through a smoothly varying atomic cross section and contains all the structural information on the local environment, to its imaginary part which is related to the density of unoccupied states in the continuum and can be expressed via a MS expansion[10] that can be used in an efficient way in data analysis to extract bond lengths and bond angles.[11,12] This equivalence will make it possible to reinterpret concepts as shape resonances in terms of MS paths followed by the final-state photoelectron on its way out of the molecular region and will substantiate the geometrical interpretation of these spectral features. At the same time the MS picture, in conjunction with the extended continuum approach, will provide a unifying scheme of interpretation for the whole absorption spectrum and will elucidate the interplay between the geometrical structure of the photoabsorbing molecule and its electronic properties.

In this paper we report analyses of the XAS spectra of the molecules SF_6, $GeCl_4$, and Br_2 following both points of view: the scattering or wave-function amplitude approach and the density of states or MS approach. Provided that the one-particle potential is real, the two points of view are mathematically equivalent and can be used interchangeably in the interpretation and description of the various spectral features. We shall also indicate the modifications needed for complex potentials. It will turn out that the two approaches are no longer equivalent in this case although they are related through a Lorentzian convolution as discussed in Sec. III. On the basis of many-body theory, a Green's-function approach, which is more akin to the density-of-states formulation, is more appropriate. We shall use the latter formulation for a "first-principles" fitting of the single-scattering and multiple-scattering (EXAFS) signals, where present, in our molecules and show that by using a complex HL exchange-correlation potential, this approach is able to reproduce EXAFS amplitudes and phases without adjustments. This finding opens the way to an *a priori* assessment of amplitudes and phases, which could in this way be fixed in a fitting procedure in order to determine with some reliability Debye-Waller factors and coordination numbers in unknown systems. Needless to say, our entire analysis has been carried out with spherical wave (SW) propagators. It has in fact been shown[13] that the usual plane-wave (PW) approximation to the SW propagators is strictly invalid in the whole energy range of the absorption spectrum although deviations are more dramatic for the low wave-vector values ($k < 5$ Å^{-1}). Therefore, in order to assess the applicability of the theory, we have chosen not to make approximations whenever possible.

II. THE SCATTERING APPROACH, THE "EXTENDED CONTINUUM" SCHEME, AND THE MS DESCRIPTION OF XAS SPECTRA

In the one-electron approximation the unpolarized photoabsorption cross section for photons with energy ω, in Rydberg units of energy and lengths, is given by

$$\sigma(\omega)=2\frac{4\pi^2}{3}\alpha\omega \sum_{L,m_\gamma,m_0} |(\psi^-_{\mathbf{k}L}| \left[\frac{4\pi}{3}\right]^{1/2} rY_{lm_\gamma}|\psi_{L_0})|^2 , \tag{2.1}$$

where $\psi^-_{\mathbf{k}L}=(\psi^+_{\mathbf{k}L})^*$ is the time-reversed[14] scattering wave function in response to an exciting free wave of angular momentum $L=(l,m)$ and ψ_{L_0} is a core-state wave function with angular momentum L_0. The factor 2 results from the spin degrees of freedom and $k=\sqrt{E}$, E being the photoelectron kinetic energy.

In the muffin-tin model both potential and solutions of the SE are represented piecewise according to the partitioning of molecular space into region I, the space enclosed by the sphere I_i of radius ρ_i around each atomic site at position $\mathbf{R}_i$, region III, the space external to the outer sphere surrounding all atomic spheres I_i, and region II, the space in between the outer and atomic spheres (interstitial region). In this way inside the atomic sphere I_i we represent $\psi^+_{k\Lambda}(\mathbf{r})$ (writing Λ for L), the scattering function in response to an exciting wave of angular momentum Λ, as

$$\psi^+_{k\Lambda}(\mathbf{r}_i)=\sum_L \widetilde{B}_L^{II_i}(\Lambda)\widetilde{f}_l^{I_i}(r_i)Y_L(\hat{\mathbf{r}}_i) ,$$

$$\mathbf{r}_i\equiv\mathbf{r}-\mathbf{R}_i\in I_i , \tag{2.2}$$

where $\widetilde{f}_l(r_i)$ is the radial solution of the SE with angular momentum l at energy E, which is regular at the origin and is normalized as indicated below.

Since the core wave function is localized in the muffin-tin sphere I_i of the photoabsorbing atom, assumed to be located at site i, we only need that part of the scattering wave function $\psi^{-}_{\mathbf{k}L}$ which is centered on I_i, so that from Eqs. (2.1) and (2.2) we obtain

$$\sigma(\omega)=2\pi\left[\frac{4\pi}{3}\right]^2\alpha\omega\sum_{\Lambda,L,m_\gamma,m_0}|\widetilde{B}_L^{II_i}(\Lambda)|^2|(\widetilde{f}_l(r_i)Y_L(\hat{\mathbf{r}}_i)|r_iY_{lm_\gamma}(\hat{\mathbf{r}}_i)|\phi_{l_0}(r_i)Y_{L_0}(\hat{\mathbf{r}}_i))|^2\ , \tag{2.3}$$

where we have replaced the dipole operator $\mathbf{r}$, referred to the center of the laboratory frame, by $\mathbf{r}_i=\mathbf{r}-\mathbf{R}_i$, due to the orthogonality between the initial and final states. If relaxation in the final state is taken into account, then the Pauli principle ensures orthogonality.

The quantity $\widetilde{B}_L^{II_i}$, giving the photoelectron wave-function amplitude inside the sphere I_i, in T-matrix normalization is also to be interpreted as a total scattering amplitude for all the waves incident on the atom located at site i coming from everywhere in the molecular region. They therefore satisfy a set of compatibility equations given by

$$\widetilde{B}_L^{II_i}(\Lambda)+t_l^i\sum_{jL'}\widetilde{G}_{LL'}^{ij}\widetilde{B}_{L'}^{II_j}(\Lambda)=-t_l^iJ_{L\Lambda}^{i0}\Gamma_\lambda\left[\frac{k}{\pi}\right]^{1/2}\ , \tag{2.4}$$

where t_l^i is the scattering amplitude of the atom located at site i for an incident wave of angular momentum L and $\widetilde{G}_{LL'}^{ij}$ the amplitude of propagation from site i to site j of a spherical wave of angular momentum L around site i and L' around site j, taking into account the distortion of the free propagation caused by the presence of the outer-sphere potential. As is well known[4(a)] one has

$$\begin{aligned}t_l^i=\exp(\delta_l^i)\sin(\delta_l^i)=&\frac{W[j_l,\widetilde{f}_l^{\,i}]}{W[-ih_l^+,\widetilde{f}_l^{\,i}]}\\=&(\text{cotg}\delta_l^i-i)^{-1}\ ,\end{aligned} \tag{2.4a}$$

where δ_l^i is the lth phase shift of the potential inside sphere I_i, $-ih_l^+=n_l-ij_l$ are, respectively, the Hankel, Neumann, and Bessel functions and $W[f,g]$ is the Wronskian of the two functions f and g calculated at the muffin-tin sphere radius ρ_i. Also

$$\widetilde{G}_{LL'}^{ij}=G_{LL'}^{ij}-\sum_{L''}J_{LL''}^{i0}t_{l''}^{0}J_{L''L}^{0j}\ , \tag{2.4b}$$

where $G_{LL'}^{ij}$ is the free amplitude propagator in T-matrix normalization which is given in Ref. 4(a). It admits the decomposition $G_{LL'}^{ij}=J_{LL'}^{ij}-iN_{LL'}^{ij}$ following the analogous decomposition of the Hankel function referred to above with $J_{LL'}^{ij}$ and $N_{LL'}^{ij}$ being defined in Ref. 2. The second term on the right-hand side (rhs) of Eq. (2.4b) represents the distortion of the free propagation due to the presence of the outer-sphere potential, centered at the origin of the coordinate frame (site 0), through the scattering amplitude [but notice the inversion with respect to Eq. (2.4a)]:

$$\begin{aligned}t_L^0=&\frac{W[-ih_l^+,-i\gamma_l]}{W[j_l,-i\gamma_l]}=\frac{W[n_l,-i\gamma_l]}{W[j_l,-i\gamma_l]}-i\\=&\cot(\delta_l^0)-i\ ,\end{aligned} \tag{2.4c}$$

where $-i\gamma_l=f_l-ig_l$ is the propagating solution of the SE in the outer-sphere potential in terms of the regular (f_l) and irregular (g_l) solutions with the proper asymptotic behavior.[2] Finally

$$\Gamma_\lambda=\frac{W[f_\lambda,-i\gamma_\lambda]}{W[j_\lambda,-i\gamma_\lambda]}\ .$$

It is easy to verify that Eqs. (2.4) in T-matrix normalization are obtained from the same equations in Ref. 2 in K-matrix normalization simply by replacing, wherever they appear, stationary waves (n_l and g_l) with the propagating ones ($-ih_l^+$ and $-i\gamma_l$). The only difference with Ref. 2 is that we have eliminated from the equations the effect of the outer sphere in favor of the physical atomic spheres, which leads to the appearance of the second term in Eq. (2.4b) as a modification of the free amplitude of propagation $G_{LL'}^{ij}$ and to the term Γ_λ on the rhs of Eq. (2.4).

Equation (2.4) simply states that the total scattering amplitude of angular momentum L at site i, $\widetilde{B}_L^{II_i}$, is equal to the atomic scattering amplitude t_l^i times the amplitude $J_{L\Lambda}^{i0}\Gamma_\lambda(k/\pi)^{1/2}$ of the exciting wave normalized to one state per Rydberg plus the scattering amplitude of all the waves that proceed from all the other atomic sites with any angular momentum, propagate up to site i arriving with angular momentum L, and are scattered by the atom at site i. In particular we want to note for future use that the inhomogeneous term Γ_λ depends linearly on the exciting amplitude f_λ in the scattering problem and therefore goes to zero when treating bound-state problems since in this case f_λ should be set to zero.

By introducing the matrix $(T_a^{-1})_{LL'}^{ij}=[(t_l^i)^{-1}]\delta_{ij}\delta_{LL'}$ diagonal in the site and angular momentum indices, one can write Eq. (2.4) as

$$\begin{aligned}\sum_{j,L'}[T_a^{-1}+\widetilde{G}]_{LL'}^{ij}\widetilde{B}_{L'}^{II_j}(\Lambda)=&\sum_{j,L'}[M-i\Delta]_{LL'}^{ij}\widetilde{B}_{L'}^{II_j}(\Lambda)\\=&-J_{L\Lambda}^{i0}\Gamma_\lambda\left[\frac{k}{\pi}\right]^{1/2}\ .\end{aligned} \tag{2.5}$$

The expression involving M and Δ comes from the decomposition of the MS matrix $T_a^{-1}+\widetilde{G}$ as $M-i\Delta$ where M and Δ are Hermitian matrices (real and symmetric if a real basis of spherical harmonics is used) such that

$$M_{LL'}^{ij}=\cot(\delta_l^i)\delta_{ij}\delta_{LL'}+(1-\delta_{ij})N_{LL'}^{ij}+\sum_{L''}J_{LL''}^{i0}\alpha_{l''}^{0}J_{L''L'}^{0j}\ , \tag{2.5a}$$

$$\Delta_{LL'}^{ij}=\sum_{\Lambda}J_{L\Lambda}^{i0}\Gamma_\lambda\Gamma_\lambda^{*}J_{\Lambda L'}^{0j}\frac{k}{\kappa}\ , \tag{2.5b}$$

with $\kappa=[E-\langle V_{II}\rangle]^{1/2}$ ($\langle V_{II}\rangle$ being the constant (volume averaged) interstitial potential) and α_1^0 the real part of $\cot(\widetilde{\delta}_1^0)$ in Eq. (2.4c).

As a consequence of their physical meaning the scattering amplitudes $\widetilde{B}_{L'}^{II_i}$ satisfy a generalized optical theorem of the form

$$\sum_{\Lambda}|\widetilde{B}_{L'}^{II_i}(\Lambda)|^2=\frac{\kappa}{\pi}\mathrm{Im}[(T_a^{-1}+\widetilde{G})^{-1}]_{LL'}^{ij}$$
$$=\frac{\kappa}{\pi}\mathrm{Im}[(M-i\Delta)^{-1}]_{LL'}^{ij} \tag{2.6}$$

which can be derived on the basis of Eq. (2.5) and the decomposition referred to above. This relation is a particular case of a theorem, valid under more general conditions, that has been proved in Ref. 4(a).

Therefore, if we introduce the atomic radial dipole matrix element

$$M_l^{l_0}=\int_0^{\rho_i}dr\, r^3\phi_{l_0}(r)R_l^i(r)\ , \tag{2.7}$$

where

$$R_l^i(r)=\widetilde{f}_l^i(r)\left[\frac{\kappa}{\pi}\right]^{1/2} \tag{2.8}$$

is the continuum regular solution of the radial SE inside sphere I_i, normalized to one state per Rydberg, that matches smoothly to

$$\left[\frac{\kappa}{\pi}\right]^{1/2}[j_l(\kappa r)t_l^{-1}-ih_l^{+}(\kappa r)] \tag{2.9}$$

at the muffin-tin radius $r=\rho_i$, one can recast the absorption cross section (2.3) as

$$\sigma(\omega)=\sigma_{l_0,l_0-1}^{a}\chi_{l_0-1}+\sigma_{l_0,l_0+1}^{a}\chi_{l_0+1} \tag{2.10}$$

by summing over m_γ and m_0.[12] Here

$$\sigma_{l_0,l_0\pm1}^{a}=\frac{8\pi^2}{3}\alpha\omega(M_{l_0\pm1}^{l_0})^2\left[\begin{matrix}l_0+1\\ l_0\end{matrix}\right]\mathrm{Im}(t_{l_0\pm1}) \tag{2.11}$$

is the dipole-allowed atomic photoabsorption cross section and

$$\chi_1=\frac{1}{2l+l}\frac{1}{\sin^2(\delta_l)}\sum_m \mathrm{Im}[(T_a^{-1}+\widetilde{G})^{-1}]_{lm\ lm}^{ii} \tag{2.12a}$$

$$=\frac{1}{2l+l}\frac{1}{\sin^2(\delta_l)}\sum_m \mathrm{Im}[(M-i\Delta)^{-1}]_{lm\ lm}^{ii} \tag{2.12b}$$

is a geometrical structure factor that contains all the structural molecular information on the environment of the photoabsorber. In Eq. (2.11) use has been made of the relation, related to the optical theorem for the atomic t matrix,[15]

$$\mathrm{Im}t_l^i=\mathrm{Im}[\exp(\delta_l^i)\sin(\delta_l^i)]=\sin^2(\delta_l^i)\ . \tag{2.13}$$

Equations (2.3) and (2.10)–(2.12) provide two alternative descriptions of the photoabsorption process which are completely equivalent mathematically. The first one may be called the scattering approach while the second can be referred to as the MS approach. Which method to use is a matter of convenience depending on the type of language one wants to utilize to describe the physics of the problem at hand and the kind of insight one wants to obtain. In the following we shall discuss the implications of both points of view trying to obtain a deeper understanding of the absorption process in molecules.

From the scattering point of view the advantage of working in T-matrix normalization is that one can treat on the same footing bound states and continuum resonances. In fact from general scattering theory[15] one knows that in the complex energy plane, bound states correspond to poles of the T matrix of the scattering potential at points on the real negative axis, whereas poles near the real positive axis in the fourth quadrant give rise to shape resonances with widths defined according to their distance from the real axis.

If we were searching for bound states such that $E<0$ but $E-\langle V_{II}\rangle>0$, we would be led to the following homogeneous equations for the amplitudes, $\widetilde{B}_{L'}^{II_i}$:

$$\sum_{j,L'}(M_b)_{LL'}^{ij}B_L^{II_j}=0 \tag{2.14}$$

which are obtained from Eq. (2.5) by setting the inhomogeneous term Γ_λ to zero as already anticipated ($f_\lambda\equiv0$, so that $\Delta=0$) and by continuing analytically the matrix M into M_b through the replacement of k by $-i\sqrt{|E|}$. Equations (2.14) have been derived in Ref. 1. For our purposes it is sufficient to note that the condition for a nontrivial solution of these equations is

$$\mathrm{Det}M_b=0 \tag{2.15}$$

which is the condition that the analytic continuation of the molecular T matrix [being proportional to $\sum_{L'}J_{LL'}^{ij}B_{L'}^{j}$ as shown in Ref. 4(a) and therefore behaving as M^{-1} according to Eqs. (2.5)] has a pole for some value or values of E on the real negative axis.

For bound states well localized in the molecular region, one anticipates that the effect of the outer sphere will be negligible [$t_l^0\cong0$ in Eq. (2.4b)], so that the condition (2.15) becomes

$$\mathrm{Det}M_0=0\ , \tag{2.16}$$

where M_0 is obtained from M in Eq. (2.5a) by dropping the outer-sphere contribution ($\alpha_l^0\equiv0$). In other words, a molecular valence state, lying above the interstitial potential, $\langle V_{II}\rangle$, which is bound in the presence of the outer sphere, shows up as a sharp resonance in the continuum when the outer-sphere potential is removed. This property holds in general for localized states, but fails to be true for extended states, e.g., Rydberg states, the existence of which depends on the presence of the outer-sphere potential. (For a discussion of Rydberg states of atoms and molecules, see Ref. 16.) The transition strengths calculated in this scheme may be wrong due to the different normalization of the continuum and bound states, however their absolute energy locations with respect to ionization threshold and relative to the other resonances in the continuum are in general accurate.

This is the essence of the extended continuum scheme. In practice one calculates a self-consistent $X\alpha$ potential for the cluster of interest, with an outer-sphere (OS) region and an OS potential. The latter is removed and a continuum calculation performed for all energies (negative and positive) greater than the constant interstitial potential $\langle V_{II} \rangle (E > \langle V_{II} \rangle)$. Notice that $\langle V_{II} \rangle$ is negative relative to the value (set to zero) of the Coulomb potential at $r \to \infty$. This approach has the advantage of calibrating on the same energy scale the bound-state features relative to the continuum features without the need to perform ionization energy calculations in order to position the bound-state transitions relative to the ionization threshold. Due to the fact that local-density calculations sometimes misrepresent excitation energies, this is not a trivial advantage. All this rests on the reasonable assumption that the correlation energies for the bound states and the continuum resonances are roughly the same.

Continuum resonances, usually within one or two Rydbergs above the ionization threshold, show up as a relative increase, around a particular energy, in the amplitude of the final-state continuum wave function of a particular symmetry at the site of the absorbing atom. The remarkable feature is that, for a given final dipole-allowed l angular momentum, the sum $\sum_{m\Lambda} |B_{lm}^{II_i}(\Lambda)|^2$ which in Eq. (2.3) determines the intensity of the transition and therefore of the absorption, is usually dominated by a single Λ value. In the case of an N_2 molecule, and in general for diatomic molecules, K-edge s-resonances are dominated by the $l=3$ term.[17(a)] In this case the amplitude increase of the wave function is ascribed to the caging effect of the centrifugal barrier in the outer-sphere region for an incoming $l=3$ partial wave as referred to the molecular center midway between the two atomic sites coupled through the molecular field to the $l=1$ photoelectron wave, as seen from the photoabsorbing site. In the literature these resonances are therefore referred to as cage or shape resonances. The concept of a centrifugal barrier has previously been thought to be general enough to encompass every case until it was found that shape resonances were possible with l values as low as 2, 1, or even 0 where clearly the centrifugal barrier cannot be effective.[18] As apparent from Eq. (2.5), which can be written as

$$-\left[\frac{\pi k}{\kappa^2}\right]^{1/2} \Gamma_\lambda B_L^{II_i}(\Lambda) = [(M - i\Delta)^{-1}\Delta]_{L\Lambda}^{ii}$$

$$= [(I - iM^{-1}\Delta)^{-1} M^{-1}\Delta]_{L\Lambda}^{ii} \qquad (2.17)$$

provided we put the origin 0 at site i so as to exploit the relation $J_{LL'}^{ii} = \delta_{LL'}$, it is clear that a sharp increase of the amplitude $B_L^{II_i}(\Lambda)$ around a particular energy E_r occurs whenever $M^{-1}\Delta$ is singular at this energy with a small residue. Since Γ_λ and the matrix elements of Δ are continuous functions of energy we again find the relation

$$\mathrm{Det} M(E_r) = 0 \qquad (2.18)$$

as a necessary condition for a resonance.[19] The other condition is that the residue at the pole should be negative and small, so that the amplitude $B_L^{II_i}(\Lambda)$ has a pole in the fourth quadrant of the complex energy plane near the real axis or equivalently, due to the relation between the T and the K matrices, that one of the eigenphases of the K matrix equation increases through $\pi/2$ by almost π in a narrow energy range around E_r.[15,17]

The condition in Eq. (2.18) encompasses the spectrum of cases for the occurrence of a shape resonance. It is a condition that links together the scattering properties of the individual atoms in the molecular cluster and their positions in space, which justifies the name cage or shape resonance given to the corresponding absorption features. For diatomic molecules or atomic clusters with only one shell at distance R from a central atom, it leads to the relation

$$(E_r - \langle V_{II} \rangle)^{1/2} R = \text{const} \qquad (2.19)$$

between the energy position of the continuum resonance and the length of the bond.[20,21] When a bound-state feature is present at energy E_b one can eliminate the interstitial potential in Eq. (2.19) to get the relation

$$\Delta E_{rb} R^2 = (E_r - E_b) R^2 = \text{const} \qquad (2.20)$$

which can be verified experimentally.[21] The condition (2.19) has also served as a basis for correlating bond lengths and shape resonances in more complicated molecules[22] or for connecting the first coordination shell distance with the energy position of the main resonance after the edge jump as has been seen in a number of compounds.[23(a)] More recently it has been used to complement EXAFS measurement of a Cu-O distance in copper-containing high-T_c superconductors.[23(b)]

However, the global information contained in Eqs. (2.19) and (2.20) does not exhaust the totality of structural information present in a molecular photoabsorption spectrum. A lot more can be learned from the expression (2.12a) for the absorption cross section. In this case the discussion of Refs. 10(b), 10(c), and 12 carries over to this case. For the convenience of the reader and for the sake of completeness we briefly summarize the conclusions. At the same time we shall try to characterize the various spectral regions of the absorption spectrum according to the rate of convergence of the MS series defined in Eq. (2.21) below, in order to have hints for performing structural analysis. From this point of view it will turn out equally interesting to analyze the concept of shape resonance in terms of diffractive interference processes connected with the MS paths involved in the resonance.

In fact, provided that the spectral radius $\rho(T_a\tilde{G})$ (maximum modulus of the eigenvalues) of the matrix $T_a\tilde{G}$ is less than one, one can perform the matrix inversion in Eq. (2.12a) by series

$$(T_a^{-1}+\tilde{G})^{-1}=(I+T_a\tilde{G})^{-1}T_a = \sum_{n=0}^{\infty}(-1)^n(T_a\tilde{G})^n T_a \qquad (2.21)$$

the series being absolutely convergent with respect to some matrix norm. In such a case one can write

$$\chi_l(k)=\sum_{n=0}^{\infty}\chi_l^n(k) \qquad (2.22)$$

where

$$\chi_l^n(k)=\frac{1}{2l+l}\frac{1}{\sin^2(\delta_l^i)}\sum_m \mathrm{Im}[(-1)^n(T_a\tilde{G})^n T_a]_{lm\,lm}^{ii} \,. \qquad (2.23)$$

This is a generalized MS expansion that reduces to the more familiar one[10,12] when the effect of the outer-sphere potential is switched off. As before $\chi_l^n(k)$ represents the partial contributions of order n in the photoabsorption coefficient of the molecule under study due to all processes in which the excited photoelectron is scattered $n-1$ times by the surrounding atoms before leaving the molecular region. Only closed scattering paths are allowed due to the site diagonal nature of Eq. (2.23). The functional form of $\chi_l^n(k)$ is given by

$$\chi_l^n(k)=\sum_{p_n}\tilde{A}_n^l(k,R_{ij}^{p_n})\sin[kR_{p_n}^{\mathrm{tot}}+\tilde{\phi}_n^l(k,R_{ij}^{p_n})] \,, \qquad (2.24)$$

where the sum is taken over all possible closed paths of order n, and $R_{p_n}^{\mathrm{tot}}$ is the corresponding path length. It is the form expected on the basis of the interference process between the outgoing and backscattered photoelectron wave at the photoabsorbing site. According to the size of the spectral radius, $\rho(T_a\tilde{G})$, one can roughly divide the photoabsorption spectrum into three energy regions.[24,25]

(1) A full multiple scattering (FMS) region, characterized by $\rho(T_a\tilde{G})\gtrsim\frac{3}{4}$, where an infinite number of paths (or a great number of them) contribute to the final shape of the absorption spectrum. For low-Z scatterers, this is usually near the edge region (1–2 Ry or 14–27 eV within the absorption edge). Only global geometrical information can be extracted from the data such as the point-group symmetry and relations of the type $\kappa R=$const. The bound-state features, whether calculated in a bound-state scheme[1] (MS-$X\alpha$) or in an extended continuum scheme clearly belong to this region. Notice that the condition Det$M=0$ for a shape resonance does not necessarily entail the inequality $\rho(T_a\tilde{G})>1$, although the spectral radius in this case should stay near the value one, since many paths interfere to create such resonances.

(2) An intermediate multiple-scattering (IMS) region characterized by $\frac{1}{2}\lesssim\rho(T_a\tilde{G})\lesssim\frac{3}{4}$, where only a limited number of paths of low order ($n\leq 4$) contribute due to the convergence of the series in Eq. (2.21). Again for small atomic clusters and according to the type of scatterers involved, this is in the approximate energy range 30 eV to 200 eV above the absorption edge. It is also the region where information on bond length is contained, since the photoelectron is sensitive to the relative position of two, three, or more atoms at a time.

(3) A single scattering (SS) region, characterized by $\rho(T_a\tilde{G})\lesssim\frac{1}{2}$, where only paths of order $n=2$ contribute significantly. This is the region where the photoelectron is sensitive only to the pair-correlation function, i.e., the relative positions of the central atom and the backscattering atom. It obviously extends into the IMS and FMS regions as well. The corresponding signal is usually referred to as EXAFS in the literature, although in proper terms EXAFS should refer to all single and MS paths signals present in the spectrum.

The general picture of a molecular absorption spectrum that emerges from the preceding discussion is one in which oscillating signals with variable amplitudes are superimposed on a background of a more or less smooth atomic absorption. In the region of convergence of the series equation, Eq. (2.21), the SS signal is strongest and acts as a carrier wave that supports all of the other MS waves.

This picture is inspiring a new kind of analysis based on a subtraction procedure for extracting the various MS signals that carry geometrical information.[12(a),25–27] In Sec. V we describe the application of the technique to SF_6, $GeCl_4$, and Br_2, in an attempt to comprehend the entire absorption spectrum within a unified scheme.

III. THE NEED FOR AN ENERGY-DEPENDENT COMPLEX POTENTIAL AND THE GREEN'S-FUNCTION APPROACH

Since the work of Lee and Pendry,[10(a)] MS theory has been widely and successfully used to interpret the modulations of the x-ray-absorption spectra in a variety of systems. These range from molecules in gas phase to adsorbates, from extended periodic systems, like crystals to disordered or amorphous materials, from large atomic clusters to small ones, both to interpret single scattering and more recently MS signals.[24–27] Used as a guide for analyzing data it becomes a powerful technique for structural analysis in many interdisciplinary fields. It is therefore of utmost importance to develop the theory further in order to eliminate the remaining discrepancies with experiments. For example, one aspect that has substantially limited the possibility of extracting reliable Debye-Waller factors (σ^2) and coordination numbers (N_i) from data is the invariable discrepancy between measured and calculated EXAFS amplitudes based on theoretical parameters (calculated amplitudes always being larger). This fact has forced and still forces investigators to simultaneously fit electronic scattering amplitudes, σ^2 and N_i to the experimental data with the risk of obtaining unreliable results in the minimization procedure ("false minima"), due to the high-statistical correlation between these parameters, or to resort to phase and amplitude transferability which is not always possible and may sometimes be dangerous. The reason for this discrepancy is the use of real potentials to calculate atomic scattering amplitudes and the consequent neglect of inelastic excitations, both intrinsic and extrinsic. These inelastic channels drain away amplitude from the elastic channel which alone gives structural information.[7] This situation calls for a many-body treatment of the photoabsorption process.

Now a formally exact solution of this problem in the language of configuration interaction or channels of the associated scattering problem is given in Ref. 28. Here however we want only to present a formal argument, based on that solution, that will enable us to achieve a reasonable guess for the one-electron potential to be used in an effective one-particle theory.

According to Ref. 28 the photoabsorption cross section can be written as

$$\sigma(\omega)=-4\pi\alpha\omega\sum_{m_0\sigma_0}\int d^3r\,d^3r'\phi_{L_0}(\mathbf{r})\boldsymbol{\varepsilon}\cdot\mathbf{r}\,\mathrm{Im}\left\{\sum_{\alpha\alpha'}S_\alpha^*S_{\alpha'}G_{\alpha\alpha'}(\mathbf{r},\mathbf{r}';\omega-I_c)\right\}\boldsymbol{\varepsilon}\cdot\mathbf{r}'\phi_{L_0}(\mathbf{r}')\ , \tag{3.1}$$

where ϕ_{L_0} is the deep-core state with angular momentum $L_0=(l_0,m_0)$ and S_α is the overlap factor $(\tilde{\Psi}_\alpha^{N-1}|\Psi_G^{N-1})$ giving, in the sudden approximation, the probability amplitude that the excited state Ψ_G^{N-1} of the spectator $(N-1)$ electrons with a core hole, created in the photoabsorption process, relaxes to the state $\tilde{\Psi}_\alpha^{N-1}$, eigenstate of the $(N-1)$ particles Hamiltonian, leaving in the system an excitation energy ΔE_α. $G_{\alpha\beta}(\mathbf{r},\mathbf{r}';E)$ is the interchannel G matrix representing the amplitude probability of propagation of the excited photoelectron from point r to point r' while at the same time the excitation energy left into the system changes from ΔE_α to ΔE_β. Due to the completeness of the $\tilde{\Psi}_\alpha^{N-1}$ states and the normalization condition $(\Psi_G^{N-1}|\Psi_G^{N-1})=1$, one has the sum rule

$$\sum_\alpha |S_\alpha|^2=1\ . \tag{3.2}$$

In Appendix C-4 of Ref. 28 it is shown that the Green's-function matrix $G_{\alpha\beta}(\mathbf{r},\mathbf{r}';E)$ satisfies the set of coupled equations

$$\sum_\gamma [(\nabla^2+\kappa_\alpha^2)\delta_{\alpha\gamma}-V_{\alpha\gamma}(\mathbf{r})]G_{\gamma\beta}(\mathbf{r},\mathbf{r}';\omega-I_c)=\delta_{\alpha\beta}\delta(\mathbf{r}-\mathbf{r}') \tag{3.3}$$

supplemented by outgoing wave boundary conditions. Here I_c is the ionization threshold of the core level, $k_\alpha^2=\omega-I_c-\Delta E_\alpha$ is the kinetic energy available to the photoelectron, ensuing a process in which the energy ΔE_α has been left into the system, and $V_{\alpha\gamma}(r)$ is the interchannel potential matrix described in Ref. 28.

This set of equations contains the complete description of all the possible outcomes of a photoemission process, be it of intrinsic origin (i.e., consequent to the relaxation of the system around the core hole) or of extrinsic origin (excitations created by the photoelectron on its way out of the system). Although the distinction between intrinsic and extrinsic losses is not in keeping with the general principles of quantum mechanics we keep it as a useful aid for classifying the system excitations according to some convenient scheme. For example, in metals and semiconductors, we might collect all the plasmon-type final channels, whether of intrinsic or extrinsic origin, which give rise to reasonably similar interchannel potential $V_{\alpha\beta}$ in Eqs. (3.3). We can then eliminate from the set of Eqs. (3.3) the Green's-function submatrix corresponding to these channels by expressing it in terms of the remaining channels. These latter are then described by a system of equations analogous to that in Eq. (3.3) having however a potential submatrix which is now complex and energy dependent due to the elimination of the plasmon channels. When the same elimination is made in Eq. (3.1) one ends up with the same expression except that the quantity inside the large curly brackets takes the form

$$\sum_{\alpha\alpha'}{}' \tilde{S}_\alpha^*(\omega)\tilde{S}_{\alpha'}(\omega)G_{\alpha\alpha'}(\omega)\ ,$$

where the overlap factors $\tilde{S}_\alpha(\omega)$ have assumed an energy dependence and the sum $\sum'$ is over the remaining channels. In particular we could eliminate all channels in favor of the completely relaxed one $(\alpha=0)$ which is the channel where the $(N-1)$ particle system remains in its possible lowest state $(\Delta E_0=0)$. This latter channel is the only one capable of giving structural information and carries most of the weight $(|S_0|^2\approx 0.7+0.8)$.[7] This procedure would lead us to a single equation for G_{00} in presence of a complex, energy dependent, nonlocal optical potential $\tilde{V}_{00}$ and to a cross section proportional to $|\tilde{S}_0(\omega)|^2\mathrm{Im}[G_{00}(\omega-I_c)]$ where $|\tilde{S}_0(\omega)|^2$ describes the effect of all the eliminated channels.

Now the construction of such a potential and the consequent solution of the effective equations for G_{00} is out of question. We can however on the basis of physical considerations try to make an ansatz as to the nature of $\tilde{V}_{00}$. For example, it is well known in fact that for metals one obtains very good agreement with the observed absorption spectra using a one-particle approach with an $X\alpha$ potential and convoluting the calculated spectrum with a Lorentzian broadening function having an energy-dependent width related to the mean-free path of the photoelectron in the system by the relation[29] $\Gamma(E)=\hbar(E/2m)^{1/2}\lambda^{-1}(E)$. The main discrepancy with experiments lies in the calculated absorption maxima falling short of the observed ones due to the energy independence of the $X\alpha$ exchange. In the framework of the above multichannel approach this finding can be rationalized by observing that in a metal the completely relaxed channel together with the plasmon excitation channels (whether intrinsic or extrinsic) almost completely exhaust the sum rule (3.2). In Si, for example, one knows that the intensity of the double-electron excitation channels is of the order 10^{-2}–10^{-3} times the main relaxed channel.[30] Therefore an optical potential given by $V_{X\alpha}+i\Gamma(E)$ is able to give a satisfactory picture of the absorption process. One can further argue that, in the spirit of a statistical approximation suggested by the opening of many channels with the same weight, the optical potential in question might be approximated by the self-energy of a uniform interacting electron gas with density given by the local density of the system under study. This fact immediately points to the Hedin-Lundqvist (HL) potential,[6(a)] with its energy-dependent exchange and its imaginary part which is able to reproduce rather accurately the observed mean-free path in metals,[31] as being a very good candidate for such an effective potential, at least for metals and semiconductors.

Although initially devised to describe exchange and correlation corrections to the Coulomb potential due to the valence charge, Lee and Beni[11] applied the HL potential to the atomic core region as well. One can therefore interpret this potential as an effective optical potential that controls the propagation and the damping of the excited photoelectron everywhere in the system. Moreover in the approximations where we can neglect excitations other than "local" plasmons, we expect $|\tilde{S}_0(\omega)|^2$ to be structureless and nearly one (to within the weight of the neglected channels). We have in this way reduced our many-body problem to an effective one-particle problem. Consequently the effective Green's function $G(\mathbf{r},\mathbf{r}';E)$ (we shall henceforth drop the index 0) will describe the propagation and attenuation of the photoelectron on its way out of the system. In keeping with the proposed interpretation, no $|\tilde{S}_0(\omega)|^2$ correction will be needed. Notice that in this way we have transferred all the weight of the plasmon intrinsic excitations to the extrinsic ones on the assumption that their effect on the absorption spectrum is similar. This fact justifies the interpretation of $G(\mathbf{r},\mathbf{r}';E)$ as a propagation amplitude described in terms of a Dyson self-energy.

The application of these ideas to the calculation of the K-edge absorption spectra of some transition metals[29] and semiconductors (ZnS, c-Si)[32] has yielded results in surprisingly good agreement with experiments. In particular, amplitudes and phases of the EXAFS oscillations are very well reproduced. What we propose here is an extension of this method of calculation (which is substantially based on a MS method with complex potentials) to the description of inner shell x-ray-absorption spectra of molecular systems. The rationale underlying this suggestion follows the same line of reasoning that led Lee and Beni[11] to extend the validity of the HL self-energy to the atomic core regions. In fact, in the spirit of the statistical approximation one might think that the relation of the HL[6] self-energy to the true self-energy of the particular system investigated is similar to that of the Thomas-Fermi approximation of the atomic density versus the shell structure obtained by solving the radial Schrödinger equation. Since many channels (of equal weight) are open in the "high-energy" region one has grounds to speculate that the above approach leads to a reasonable description of the EXAFS oscillations in an absorption spectrum. On the other hand, in the near-edge region of the spectrum (below and above the ionization threshold), one does not expect to reproduce all of the absorption features. (This is due to the discrete nature of the channels open for excitation.) One will obtain an average one-particle background onto which real many-electron features will be superposed. Single-particle resonances could then be separated from multiparticle excitations. We shall encounter an example of this situation in the analysis of the SF_6 spectrum.

As a result of the reduction described above, the function $G^+(\mathbf{r},\mathbf{r}';E)$ obeys an effective one-particle Schrödinger equation, better known as Dyson's equation, given by

$$[\nabla^2+E-V_c(\mathbf{r})-\Sigma_{\mathrm{exc}}(\mathbf{r};E)]G^+(\mathbf{r},\mathbf{r}';E)=\delta(\mathbf{r}-\mathbf{r}') , \tag{3.4}$$

where $\Sigma_{\mathrm{exc}}(\mathbf{r};E)$ is the local energy-dependent, complex HL[6] exchange and correlation potential, and V_c is the usual Coulomb or Hartree potential.

The result is consistent with the physical picture of the photoabsorption process, in which we add an electron to the ground state of the $(Z+1)$ equivalent atom. Therefore $G(\mathbf{r},\mathbf{r}';E)$ describes the propagation of the excited photoelectron from point $\mathbf{r}$ to point $\mathbf{r}'$. The amplitude of this propagation is the probability amplitude that the added electron remains in the original state in which it has been added to the system. Its imaginary part, as in the scattering case, gives the total probability of scattering out of the initial state. As a result, mean-free path effects are automatically taken into account in this way, as discussed in detail in Ref. 32.

Equation (3.4) is to be solved with outgoing wave boundary conditions for G^+ and the solution is readily obtained for a collection of muffin-tin potentials.[33] Due to the localization of the core state $\phi_{L_0}(\mathbf{r})$ at the photoabsorbing site i in Eq. (3.1) we need the solution of Eq. (3.4) only for $\mathbf{r},\mathbf{r}'\in I_i$, the sphere around the excited atom. Taking the origin at site 0, this solution is

$$G^+(\mathbf{r},\mathbf{r}';E)=-\sum_{LL'}R_L(\mathbf{r})\tau^{00}_{LL'}R_{L'}(\mathbf{r}')+\sum_{L}R_L(\mathbf{r}_<)S_L(\mathbf{r}_>) \tag{3.5a}$$

$$=-\sum_{LL'}R_L(\mathbf{r})[\tau^{00}_{LL'}-t^0_1\delta_{LL'}]R_{L'}(\mathbf{r}')-\sum_{L}R_L(\mathbf{r}_<)t^0_lR^+_L(\mathbf{r}_>) , \tag{3.5b}$$

where $R_L(\mathbf{r})=R_l(r)Y_L(\hat{r})\equiv(\kappa/\pi)^{1/2}\tilde{f}_l(r)Y_L(\hat{r})$ is again that solution of the Schrödinger equation inside I_0, regular at the origin and matching smoothly to

$$\left[\frac{\kappa}{\pi}\right]^{1/2}[j_l(\kappa r)t_l^{-1}-ih_l^+(\kappa r)]Y_L(\hat{r}) \tag{3.6}$$

at $r=r_0$, the muffin-tin sphere radius. Here and below $\mathbf{r}_{<(}\mathbf{r}_{>)}$ is the lesser (the greater) of $|\mathbf{r}|$ and $|\mathbf{r}'|$. Similarly, $S_L(\mathbf{r})=S_l(r)Y_L(\hat{r})$ and $R_L^+(\mathbf{r})=R_l^+(r)Y_L(\hat{r})$ are solutions of the Schrödinger equation in I_0, singular at the origin and matching smoothly to $(\kappa/\pi)^{1/2}j_l(\kappa r)Y_L(\hat{r})$ and $-i(\kappa/\pi)^{1/2}h_l^+(\kappa r)Y_L(\hat{r})$, respectively, at $r=r_0$. These terms account for the singular part of the Green's function $G^+(\mathbf{r},\mathbf{r}';E)$. Due to the relation (3.6), one also has

$$R_L(\mathbf{r})=S_L(\mathbf{r})(t_l^0)^{-1}+R_L^+(\mathbf{r})$$

so that Eq. (3.5b) follows from Eq. (3.5a). Moreover τ is the scattering path operator given by

$$\tau_{LL'}^{00}=[(T_a^{-1}+\tilde{G})^{-1}]_{LL'}^{00} , \tag{3.7}$$

where T_a and $\tilde{G}$ are the same as in Eq. (2.5). In Ref. 33, the solution (3.5a) is given for real muffin-tin potentials without an outer sphere. In a real spherical harmonic basis, which we use, the solution can be shown to be valid for complex potentials and in the presence of an outer sphere, as well. In this last case however, R_L and S_L are obviously complex.

Insertion of the solution (3.5b) into Eq. (3.1) written only for channel 0 without the $|S_0(\omega)|^2$ factor as illustrated above, gives the polarization averaged cross section

$$\sigma(\omega)=\frac{8\pi^2}{3}\alpha\omega\sum_{lm}A(l_0,l)\text{Im}\{M_l^{1_0}[\tau_{lm\ lm}^{00}-t_l^0]M_l^{l_0}+M_l^{l_0}t_l^0\overline{M}_1^{l_0}\} , \tag{3.8}$$

where $M_1^{1_0}$ is the same as defined in Eq. (2.7),

$$\overline{M}_1^{1_0}=\int\int dr\, r'^3dr'\phi_{l_0}^c(r)R_L(r_<)R_L^+(r_>)\phi_{l_0}(r')/M_l^{l_0}$$

and

$$A(l_0,l)=\delta_{l,l_0-1}\frac{1_0}{2l+1}+\delta_{l,l_0+1}\frac{l_0+1}{2l+1} .$$

Only for real potentials does this expression reduce to the more familiar formula (2.10)[10,12]

$$\sigma(\omega)=\frac{8\pi^2}{3}\alpha\omega\sum_{lm}A(l_0,l)(M_l^{l_0})^2\text{Im}\tau_{lm\ lm}^{00} \tag{3.9}$$

which follows from Eq. (3.5a) by noticing that in this case R_L and S_L are real functions. The atomic absorption $\sigma_a(\omega)$ is obtained by putting $G\equiv 0$ in Eq. (3.14):

$$\sigma_a(\omega)=\frac{8\pi^2}{3}\alpha\omega\sum_{lm}A(l_0,l)\text{Im}\{M_l^{l_0}t_l^0\overline{M}_l^{l_0}\} , \tag{3.10}$$

whereas the effect of the structure is contained in the multiple-scattering series

$$\sigma_s(\omega)=\frac{8\pi^2}{3}\alpha\omega\sum_{lm}A(l_0,l)\sum_{n=0}^{\infty}\text{Im}\{(M_l^{l_0})^2(t_1^0)^2[(-1)^n\tilde{G}(T_a\tilde{G})^n]_{lm\ lm}^{00}\}=\sum_{n=0}^{\infty}\sigma_s^n(\omega) \tag{3.11}$$

which is obtained by expanding the scattering path operator τ in series as in Eq. (2.21).

Notice that in the complex potential case the atomic cross section (3.10) does not factorize out from the structural contribution (3.11) as was the case for real potentials in Eqs. (3.9) and (2.10). Therefore in view of the experimental analysis we define

$$\chi_l(\omega)=\frac{\sigma_l(\omega)}{[\sigma_a(\omega)]_l}-1 \tag{3.12a}$$

for the total fine-structure signal in channel l and

$$\chi_l^n(\omega)=\frac{\sigma_l^n(\omega)}{[\sigma_a(\omega)]_l} \tag{3.12b}$$

for the various MS signals of order n in channel l.

As shown in Ref. 32 and verified for the calculations presented in the following sections, a real potential calculation followed by a Lorentzian convolution with an energy-dependent broadening function equal to the imaginary part of the complex potential reproduces the results obtained via the solution of Dyson's equation (3.4) for the photoelectron Green's function with complex self-energy and then using Eqs. (3.10)–(3.12). Therefore, modulo a Lorentzian convolution, we can still use the scattering approach as a viable description of the photoabsorption process even though the many-body approach would lead to a MS description.

IV. SF_6 EXPERIMENTAL METHODS

The sulfur K-edge absorption measurements of SF_6 were performed at the Stanford Synchrotron Radiation Laboratory using the SSRL/LBL/EXXON 54-pole wiggler beam line 6-2 operated in focused undulator mode with a magnetic field of 5 kG. The sample fluorescence signal was measured using a N_2-filled detector of Stern-Heald[34] design onto which a gas flow cell was adapted. The sample used in the measurements consisted of a gas mixture of 2:1 He to SF_6 by volume. Two slits were used to define the beam and a He-filled ion chamber was used to measure I_0. The experimental resolution ($\approx$0.5 eV), was determined by the Darwin width of the Si(111) monochromator crystals and the vertical divergence of the x-ray beam.[35] Energy calibration was done by assigning the first peak in the sulfur *K*-edge spectrum of a calibration sample of $Na_2S_2O_3 \cdot 2H_2O$ to 2472.0 eV which results in a first-inflection point at 2471.3 eV in a powdered sample of elemental sulfur. The calibration samples were run before and after measurement of the gas spectra of SF_6. Data analysis followed the standard procedure[36] of normalization of the post-edge region to unity, after subtraction of the pre-edge region, based on a spline fits in the post-edge and polynomial fits in the pre-edge region. The data presented represent the average of two 40-min scans.

V. APPLICATION OF GENERAL METHODS TO SF_6

Since the publication in 1966 (Ref. 37) of the gas phase sulfur *K*-edge photoabsorption spectrum of SF_6, the "unusually rugged" spectral profile from the S 1*s* threshold at 2490 eV up to about 2570 eV has attracted the interest of many researchers. Figure 1(a) shows the spectra recorded at SSRL and fixes the notation of the various spectral features as used by Ferrett *et al.*[38] and Gianturco *et al.*[39] except that in this last paper features *F* and *G* are interchanged.

Zimkina and Vinogradov[40(a)] made an early attempt to interpret the *K*-edge spectrum based on aligning the S 1*s*, S 2*p*, and F 1*s* photoabsorption spectra in SF_6 along the respective ionization thresholds. From the observed similarity of the spectra it was concluded that the prominent features were due to "transition of the core electron to some common system of excitation states." By relying on a schematic molecular orbital (MO) diagram for SF_6 with four unoccupied orbitals [$a_{1g}(3s)$, $t_{1u}(3p)$, $t_{2g}(3d)$, and $e_g(3d)$] Zimkina and Vinogradov[40(a)] were able to assign feature *A* to a dipole-forbidden transition to the a_{1g} state and feature *B* to the dipole-allowed transition to the

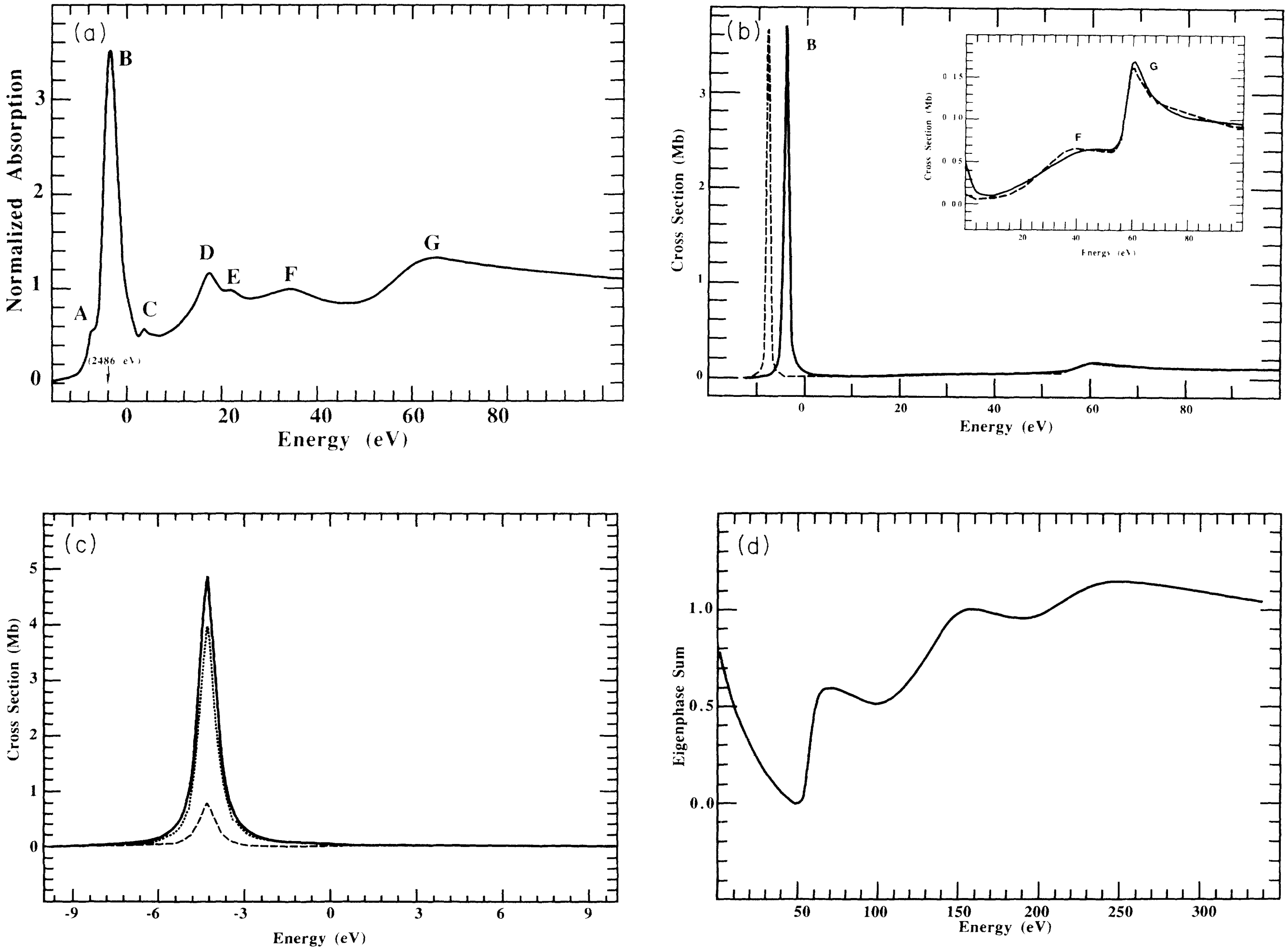

FIG. 1. SF_6 near edge (FMS) and IMS regions: (a) The measured edge spectrum. (b) The edge spectrum computed by the extended continuum method (solid line) and via an explicit bound-to-bound state calculation combined with a real HL potential computed using an outer sphere for the region $E > 0$ (dashed line). (b inset) The blown-up continuum part of the computed spectrum. (c) The l decomposition of the bound-state resonance computed via the EC-MS-$X\alpha$ scheme. The solid line is total cross section (first 9 basis functions) while the dashed and dotted lines correspond to $l = 1$ and $l = 3$ components, respectively. (d) Eigenphase sum [Eq. (6.3)] for the continuum part of the spectrum in units of π.

t_{1u} state both situated below the ionization threshold (IT). Zimkina and Vinogradov[40(a)] concluded that the concept of potential barrier put forward by Nefedov[41] to explain the presence of sharp continuum resonances in the S L_{II}-L_{III} edge spectrum could not be used for the S K edge to explain features C and D above the IT as $1s \rightarrow t_{2g}, e_g$ transitions on the basis that these features were also present in the K-edge spectrum of fluorine. Nearly at the same time and independently of them, Dehmer[40(b)] used the same potential barrier idea supplemented by a double-well molecular potential model to assign the continuum features C and D to vibronically assisted transitions to the t_{2g} and e_g states due to the photoelectron being trapped in the inner potential well by an effective barrier of 8 and 20 eV, respectively. Dehmer[40(b)] bypassed the objection by Zimkina and Vinogradov[40(a)] by the assumption that in the F K edge the outer-well states overlap less effectively with the core levels of F than do the inner-well states. Following this interpretation, since all the continuum resonances in the S K spectrum occur at unusually high-photoelectron kinetic energy, SF_6 has become a prototypical example of potential barrier and shape resonance effect. Dehmer[40(b)] also confirmed the assignment, given in Ref. 40(a), of features A and B below the IT as transitions to the antibonding states a_{1g}, and t_{1u}, the a_{1g} transition being vibronically assisted. Finally feature E was interpreted as marking "the onset of direct ionization which begins where the kinetic energy of the photoelectron surpasses the potential barrier height" of 20 eV that keeps the excited electron of feature D inside the inner well.

While these interpretations were qualitative in character, quantitative explanations date from the same period. Led by the idea that the prominent features in the absorption spectrum represent transitions to unoccupied orbitals strongly localized in the molecular region, Gianturco *et al.*[39] attempted to understand the continuum resonances as electronic excitations into virtual orbitals with antibonding character embedded in the continuum obtained via an LCAO MO calculation. The assignment arrived at was the same as suggested in Ref. 40(a) for features A, B, and C with a good agreement between calculated and experimental energy spacings. Feature D however was assigned to a dipole-allowed transition to a MO state of t_{1u} symmetry, 2 eV above the C feature, in marked contrast with the experimental value of 13 eV. Feature E was instead assigned to a dipole-forbidden transition to a state of e_g symmetry with the correct energy spacing from feature C (18 eV). The features at higher energies (F, G, and the undulatory structure above) were interpreted as due to double-excitation processes, as was the broadening of feature D. Clearly the level structure recommended in Ref. 40(b) and later confirmed by the experimental results for photoelectron branching ratios and angular distributions was not reproduced.[42]

However a similar recent calculation based on the discrete-variational $X\alpha$ MO calculations of virtual orbitals by Nakamatsu *et al.*[43] has reproduced the level structure recommended in Ref. 40(b) with the correct energy spacing for the four features A, B, C, and D, which have therefore been given the same assignment suggested in Ref. 40(b). Nakamatsu *et al.*[43] suggest that these resonances originate from the "constructive interference between the wave function in the central sulfur atom and that scattered by the surrounding fluorine atoms." They further noted the absence of any potential barrier in the molecular potential as shown from a cross-sectional plot along the F-S-F direction.

The weak point in the interpretations reported above lies with the assignment of the strong feature D to a dipole-forbidden transition which should therefore be vibronically assisted. Empirically, the intensity of vibronically assisted dipole-forbidden transitions is approximately 10% or less than that of the main line which is not the case for feature D.[44] Additionally, features A and C have yet to be treated rigorously from the computational point of view. We defer the proper treatment of vibrational and multielectron effects to future work. Finally the assignment of features F and G, attempted only in Ref. 39, to double-electron excitations is rather without quantitative support and is not convincing.

In 1986 the problem of the interpretation of the S K-edge photoabsorption spectrum has been addressed from the experimental point of view by Ferrett *et al.*,[38] who have measured the photoelectron spectrum between 2460 and 2600 eV across the discrete and continuum resonances in the vicinity of the S K edge. From a study of the decay of the various resonances they were led to the conclusion that features D and E should be assigned to doubly excited autoionizing states with configuration $1s^{-1}v^{-1}t_{1u}v^*$ in a MO picture (v and v^* being occupied and empty valence states, respectively) which were observed to decay into S $2p$, S $2s$, and/or valence photoemission channels. They noted that the threshold for the satellite $1s \rightarrow$continuum lies 3–4-eV higher than features D and E. They also noted that at photon energies between 2520 and 2570 eV, the large oscillations of the S $1s$ cross section is well reproduced by the MS-$X\alpha$ calculation performed by Wallace,[45] but an attempt at explaining the oscillations in terms of single-scattering diffractive effects using a plane-wave approximation was not satisfactory. Ferrett *et al.*[38] concluded that "improvements in the description of both the electron scattering and the molecular potential are necessary to model the diffractive (EXAFS-like) and nondiffractive (barrier interaction) effects in this energy region."

It was therefore very natural for us to try to make a contribution to the understanding of the S K-edge spectrum in gas phase SF_6, since our approach describes both points of view (diffractive and barrier effects) in a unifying scheme. The analysis of the spectrum of SF_6 was therefore performed using the general principles and approach described in the preceding sections.

A. Analysis based on the scattering approach

In Fig. 1(a) we show the measured spectrum corresponding to the energy interval from -12 to 70 eV and containing all of the relevant features labeled A through G with the same notation used in Ref. 38. The zero of energy here and in the following corresponds to the ionization threshold I_0 as determined experimentally by Ferrett

TABLE I. Structural and computational information for SF_6, $GeCl_4$, and Br_2.

Molecule	$R_{\mathrm{bond}}(a_0)^{\mathrm{a}}$	DW Fct. $(a_0^2)^{\mathrm{a}}$	$R_{\mathrm{osp}}(a_0)^{\mathrm{b}}$	$R_{\mathrm{cent}}(a_0)^{\mathrm{b}}$	$R_{\mathrm{lig}}(a_0)^{\mathrm{b}}$
SF_6	2.95	0.006 18	4.53	1.68	1.57
$GeCl_4$	3.99	0.007 25	6.07	1.91	2.08
Br_2	4.31	0.007 08	4.31	2.15	2.15

[a] The bond distances (R_{bond}) and Debye-Waller factors (DW Fct.) are in atomic units and were taken from Refs. 50 (SF_6), 61 ($GeCl_4$), and 7 (Br_2), respectively. Of the DW factors used, only that for Br_2 was not an experimental value.

[b] Note that the outer sphere and interstitial potential α values were obtained via a direct average of the atomic values determined by Schwarz (Ref. 52) and were set equal. Also, all sphere radii were determined by the Norman method (Ref. 51) and, except for SF_6 which has 10% overlap of the atomic spheres, the spheres are constructed to touch with no overlap. The sphere radii of absorbing atom (cent), ligand atoms (lig), and outer-sphere (osp) region are given.

et al.[38] As we shall show below, in this energy interval the calculated spectral radius $\rho(TG)$ is ≥ 0.75, characterizing this portion of the spectrum as a full multiple scattering region. Moreover, the region where $\rho(TG)$ is ≥ 0.7 extends as far as 130 eV above threshold reflecting the strong scattering power of S and F atoms.

Figure 1(b) shows (solid line) the results of an extended continuum MS calculation which uses the real part of the HL exchange and correlation potential for dipole-allowed transitions from a 1*s* S core state of a_{1g} symmetry to a continuum final state of t_{1u} symmetry. The dashed line shows the results of a similar calculation which uses the standard approach of computing the dipole cross section for a final bound state of t_{1u} symmetry combined with a continuum calculation utilizing a real HL potential. An outer sphere is present both for the bound and continuum cases. We refer the reader to Table I for information on MT radii used.

Before discussing in some detail the differences and similarities of the two methods, we note that in both cases only features *B*, *F*, and *G* are reproduced in the MS calculations of dipole-allowed transitions to bound or continuum final states.

The assignment of the only intense peak below threshold as a S 1*s* to $6t_{1u}$ level is straightforward. In the standard approach the cross section for bound-to-bound transitions is calculated using the bound-state version of Eq. (2.1) given by[8]

$$\sigma(\omega)=\frac{8\pi^2}{3}\alpha\omega\sum_{L,m_\gamma,m_0}\left|\left(\psi_L^b\left|\left[\frac{4\pi}{3}\right]^{1/2}rY_{1m_\gamma}\right|\psi_{L_0}^c\right)\right|^2\frac{(\gamma/2\pi)}{(\omega-\omega_L)^2+(\gamma/2)^2}\,, \tag{5.1}$$

where ψ_L^b is the bound final-state component (valence level), centered on the sphere of the absorbing atom of symmetry t_{1u} of the point group O_h allowed by the dipole selection rule, γ is the core hole lifetime [which is 0.59 eV (Ref. 46) at the S *K* edge], and ω_L is the transition energy (2486 eV).

The calculated value of ~ 3.6 megabarns (Mb) for the cross section compares favorably with the value of ~ 1.9 Mb reported in Ref. 38. When correcting for an experimental resolution of 0.25 eV, one obtains $\sigma(\omega_L)=3.6\times 0.59/(0.59+0.25)=2.5$ Mb, since $\sigma(\omega)$ scales as $1/\gamma$. In order to carry out this calculation the following had to be done.

(1) Computation of a self-consistent-field-scattered wave $X\alpha$ (SCF-SW-$X\alpha$) ground-state potential, with which to calculate the one-electron initial states.

(2) Computation of a spin-polarized SCF-SW-$X\alpha$ final-state potential in the configuration $1s^{-1}6t_{1u}$. (That is to say, the SCF spin-up 1*s* to spin-up $6t_{1u}$ configuration.)

(3) Computation of the dipole cross section for the transition $1s \rightarrow t_{1u}$, using the one-particle states relative to the ground-state and excited-state potentials, respectively. In doing so, we neglect the effect of the nonorthogonality of the wave functions of the passive electrons in the initial and final states. This fact might account for the discrepancy between the calculated and experimental values. By calculating the SCF-SW-$X\alpha$ final state, relative to the charged configuration $1s^{-1}$ with a 1*s* core hole and taking the total energy difference between this state and the one relative to the configuration $1s^{-1}6t_{1u}$, we have computed the term energy ΔE_{tot} ($\Delta E_{\mathrm{tot}}=7.7$ eV). This means that the 1*s* ionization threshold is 7.7 eV above the transition, whereas the measurements of Ferrett *et al.*[38] yielded 4 eV. This discrepancy is not surprising for local density calculational schemes. By following the same convention used for the experimental spectra we also let the ionization threshold in the calculated spectra coincide with the zero of the energy scale, which is also the zero of photoelectron kinetic energy.

In the standard approach the continuum cross section is calculated in the manner of Dill and Dehmer,[2] using an outer sphere and real potentials. The result of this calculation is plotted as the dashed line in Fig. 1(b). The same analysis can be carried out in the EC-MS-RHL in a manner which is mathematically more elegant and computationally faster than the standard approach. The result is shown as the solid line in Fig. 1(b) and was obtained using the same molecular potentials as in the standard calculation but without the outer-sphere potential.

Using the SCF Coulomb potential (as obtained from the total charge density) and the spin-up charge density already obtained from the excited configuration $1s^{-1}6t_{1u}$ to calculate the exchange and correlation parts of the real HL potential, the total cross section in both the bound and continuum regions was computed as a single continuum cross section. It should be noted that here the zero of energy is the zero of the Coulomb potential at infinity and should be interpreted as the ionization threshold. Therefore, in this approach the term value for the $1s \rightarrow t_{1u}$ turns out to be 4 eV in keeping with the experimental value of Ferrett *et al.*[38] The extended continuum method has two drawbacks but several advantages. As a result of using a continuum final-state normalization in the bound-state region the calculated intensities might not be correct [the good agreement with the explicit bound-to-bound computation seen in Fig. 1(b) is incidental and should not be taken as the general case]. In addition, removal of the outer-sphere potential results in the inability to properly handle Rydberg states which depend strongly on the boundary conditions imposed on the wave functions. On the other hand, some of the advantages include speed of computation, rather accurate energy spacings, and the possibility of decomposing the bound-state features according to the l values of the incoming spherical waves.

The computational advantage can already be seen. In order to compute all bound-state transition intensities for a final state transforming under a given dipole-allowed irreducible representation, only one SCF final-state potential need be computed. Concerning the second point, note that in the particular case of the SF_6 molecule that the energy spacing Δ_{BG} between features B and G in Fig. 1(a) is not well reproduced in the EC scheme. This scheme gives a value of 64 eV compared with 68 eV found experimentally. However, the agreement achieved by the standard calculation is fortuitous, since it is based on an estimate of the term value for the B transition (7.7 eV as opposed to 4 eV). Also note that the two calculations with and without an outer-sphere potential are nearly coincident. The third advantage lies in the fact that the EC method, by treating the bound states as continuum resonances, makes possible the decomposition of the total cross section in terms of the partial contributions of the various asymptotic incoming spherical waves as given by Eq. (2.3):

$$\sigma_{\mathrm{tot}}(\omega)=\sum_{\Lambda}\sigma_{\Lambda}(\omega) \ . \tag{5.2}$$

We see in Fig. 1(c) that the bound-state feature B can be represented as a scattering resonance dominated by the $l=3$ (dotted line) and to a lesser extent by the $l=1$ (dashed line) partial waves. (It should be noted that because of the presence of ligands, the full spherical symmetry about the absorbing site is broken and hence channels other than the exciting channel are available to the incoming photoelectron.[2]) This information on the nature of the molecular potential can be used to supplement that coming from possible shape resonances in the continuum.

In order to understand the physical origin of features F and G we calculated the eigenphase sum μ_{sum} defined as[17]

$$\mu_{\mathrm{sum}}=\delta_{\mathrm{sum}}/\pi=\frac{1}{\pi}\sum_{\Lambda}\tan^{-1}(U^TKU)_{\Lambda\Lambda} \ , \tag{5.3}$$

where U is the real, orthogonal matrix which diagonalizes the real symmetric K matrix. In Fig. 1(d) the eigenphase sum for the final eigenchannel of t_{1u} symmetry has been plotted. [It should be noted that the curve was made continuous by imposing the restriction $0 \leq \mu_{\mathrm{sum}} \leq 1$ and shifting all branches of $\tan^{-1}(x)$ into this region.] As already discussed by Dehmer and Dill,[17] "the eigenphase sum is a fingerprint in multichannel scattering processes which indicates any rapid changes in phase of a major partial wave component of the final-state wave function."

We see from Fig. 1(d) that the eigenphase sum increases by $2\pi/3$ over an energy range of about 10 eV centered around feature G at 60 eV. Hence it is tempting to consider this feature as a shape resonance, since it has the same behavior as that found in the N_2 σ_u channel although at a much lower energy (approximately 10 eV photoelectron kinetic energy).[17] The problem in the case of SF_6 is that it is difficult to imagine the physical origin of the required barrier height (approximately 65 eV) needed to trap the photoelectron. However there are other arguments in support of this assignment. First, of all, as we show below, at this energy the value of $\rho(TG)$ is around 1, indicating that it is a FMS resonance. In other words an infinite or large number of MS signals contribute to its shape by constructively interfering at a particular photoelectron energy. In fact the shape of the feature G is very reminiscent of the first absorption peak in the K-edge spectra of transition metal-ion salts in aqueous solution, which coordinate with six water molecules to form octahedral complexes.[12(a),47] It seems that in the case of SF_6 we are in the presence of a "delayed octahedral resonance" pushed up in energy by 60 eV. Secondly, and more importantly, from the unifying scheme presented above, the distinction between the two physical origins of a spectral feature (diffraction as opposed to barrier effects) is somewhat less sharp than previously thought. We have in fact shown that any resonance can be decomposed into MS signals originating from a number of geometrical paths, followed by the photoelectron in its final state. What distinguishes a resonance from a "diffractive" maximum in the cross section is therefore the number and coherence of the "diffractive" signals contributing to the spectral feature under consideration. In a resonance, the many "diffractive" signals interfere coherently giving rise to a sharp feature while in a "diffractive" maximum only a few "diffractive" signals (in some cases only one) contribute with little or no coherence. It is also possible to realize a large spectrum of intermediate cases between both extremes. Thirdly, it has been shown[19] that one does not need a "barrier" effect to have a resonance since the concept of a potential resonance is more general than the barrier model. Based on all of these considerations we therefore assign feature *G* to a "delayed octahedral shape resonance." As shown below, the introduction of an absorptive part in the HL potential (imaginary part of the Dyson self-energy $\sum_{\mathrm{exc}}$ [see Eq. (3.10)]) to account for the finite lifetime of the photoelectron in the final state reduces the value of the convergence parameter $\rho(TG)$ to approximately 0.75 and improves the convergence of the MS series. We shall therefore attempt a decomposition of the feature *G* into MS paths.

More problematic is the assignment of feature *F*. From the fact that it falls in an energy region where the eigenphase sum *decreases* by approximately $3\pi/4$ over an energy range of 50 eV, we are led to refer to it as an antiresonance. In other words, the scattering is strong but there is no real trapping of the photoelectron wave in the potential region. In our calculation the energy spacing Δ_{FG} between features *F* and *G* is not very well reproduced: 20 eV as opposed to the experimental value of 30 eV. It should be noted that this spacing depends strongly on the details (e.g., MT radii) of the potential. Moreover, it is also sensitive to the presence or absence of an outer-sphere potential. The MS calculations of Wallace[45] quoted in Ref. 38 is in better agreement with the experimental data ($\Delta_{FG}=25$ eV). We believe that any differences are due to the choice of sphere radii. (The radii used by Wallace[45] were $r_{\mathrm{osp}}=4.21$, $r_{\mathrm{cent}}=1.76$, and $r_{\mathrm{lig}}=1.22$, all in atomic units.) The general shape of the two calculated spectra is very similar however. Consequently we are rather confident in the one-electron nature of feature *F*.

In order to enhance our understanding of this part of the energy spectrum we examine the asymptotic partial wave decomposition of the total cross section in terms of the partial cross sections $\sigma_\Lambda(E)$ [see Eq. (5.2)] corresponding to the outer sphere (and central atom) first seven basis functions of the symmetrized t_{1u} final state. In Figs. 2(a) and 2(b) we display the contributions for the $l=1$ [Fig. 2(a) solid line], $l=3$ [Fig. 2(a) dashed line], $l=5$ [Fig. 2(a) dotted line], $l=5$ [Fig. 2(a) dot-dashed line], $l=7$ [Fig. 2(b) solid line], $l=7$ [Fig. 2(b) dashed line], and $l=9$ [Fig. 2(b) dotted line]. The states with the same l values are orthogonal states transforming according to the t_{1u} representation. The functions $\sigma_\Lambda(E)$ were computed via the EC-MS-$X\alpha$ scheme. In Fig. 2(c) we also display the total cross section (nine basis functions, solid line) with the sum of contributions of the first four basis functions (dashed line) and of the first seven basis functions (dotted line).

We note that in the region of the *G* resonance, the partial wave contributions corresponding to $l=5$, $l=7$ (both states) and $l=9$ partial waves resonate. This is akin to what has been observed in the N_2 molecule where only the $l=3$ partial wave resonates.[17(b)] Consequently, feature *G* might be called a centrifugal barrier resonance, although this name, as for the case of N_2 does not explain why the resonance happens to fall at that particular energy. We also note the interference effect in the $l=1$ and in the $l=3$ eigenchannel between features *F* and *G*, due to an interplay of background eigenphases. This can be considered as confirmation of the assignment of *F* to an antiresonance.

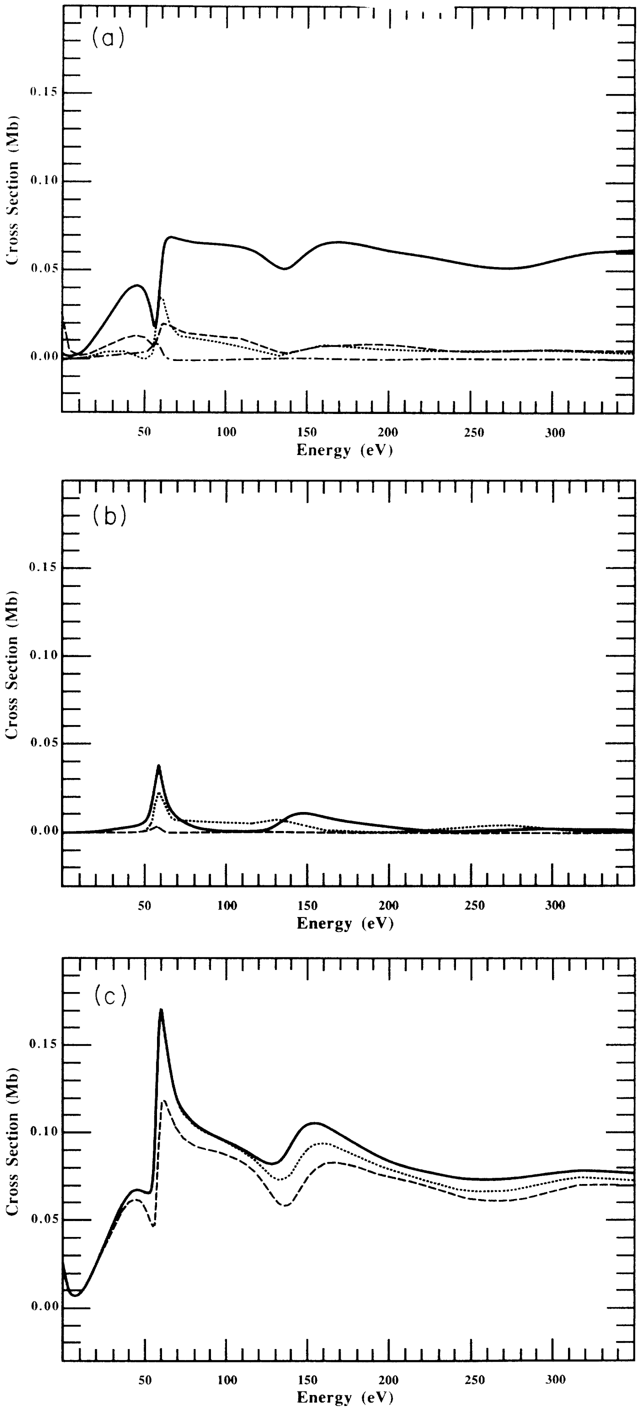

FIG. 2. SF_6 FMS, IMS, and SS partial wave decomposition: (a) Partial cross sections for basis functions with $l=1$ (solid line), 3 (dashed line), 5 (dotted line), and 5 (dot-dashed line). (b) Partial cross sections for basis functions with $l=7$ (solid line), 7 (dashed line), and 9 (dotted line). (c) Total cross-section (solid line) sum of first four basis functions (dashed line) and sum of first seven basis functions (dotted line).

B. Energetics of multielectron transitions

Returning to the other features, we noted above that the MS approach fails to account for the features labeled *A*, *C*, *D*, and *E* in Fig. 1(a). Since our computational scheme deals with only electronic excitations, it cannot handle vibronically allowed transitions. Therefore we cannot discriminate between the assignments for features *D* and *E* made by Dehmer[40(b)] and Ferrett *et al.*[38] or be more positive about the interpretation of features *A* and *C*. Based on the work of Ferrett *et al.*,[38] and noting that features *D* and *E*, taken together, seem to be an enhanced replication of feature *C* which is then split into a strong peak followed by a weaker one [see Fig. 1(a)] we are inclined to assign all of them to double electron transitions.

Having performed a SCF-MS-$X\alpha$ calculation for the configuration $1s^{-1}6t_{1u}$ we are in a position to study the energetics of double electron transitions. Table II shows the single-particle spin-polarized valence levels for this configuration. Although in general single-particle energy spacings do not give the correct excitation energies, we have checked that the total energy differences between the appropriate SCF configurations give substantially the same values. Therefore we have chosen to present the single-particle levels in Table II as an aid to intuition.

In the sudden approximation the intensities of double excitations are governed by the monopole matrix elements between the spectator states in question.[48] (See Ref. 49 for a more complete discussion of the general problem of multielectron excitation from both the theoretical and the experimental perspectives.) So we expect the strongest transitions to be the ones with the maximum overlap between the final and initial states of the passive electron. On physical grounds we expect this transition to screen the S 1*s* core hole, so that in the final state there should be more charge on the S MT sphere than there is in the initial state. The only passive electron transition satisfying these requirements is the $4t_{1u} \rightarrow 6t_{1u}$ transition, so that the final state has the configuration $1s^{-1}4t_{1u}^{-1}6t_{1u}^{2}$, corresponding to bonding and antibonding molecular orbitals of 3*p*(S)-2*p*(F) character. This configuration lies approximately 17 eV above the one-electron configuration $1s^{-1}6t_{1u}$ and should be identified with feature *D* lying approximately 20 eV above feature *B*.

We find a similar situation for the bonding-antibonding pair 3*s*(S)-2*p*(F) corresponding to the passive electron transition $5a_{1g} \rightarrow 6a_{1g}$, however this is an antiscreening

TABLE II. Valence level scheme for the spin-polarized $1s \rightarrow t_{1u}$ excited-state potential of SF_6.

Level[a]	Occupancy	Character[b]	Energy (eV)	Spin
$1T_{1g}$	3.0	2*p*(F)	−16.2969	↑
$1T_{1g}$	3.0	2*p*(F)	−16.1350	↓
$1T_{2u}$	3.0	2*p*(F)	−14.6866	↑
$1T_{2u}$	3.0	2*p*(F)	−14.5037	↓
$4A_{1g}$	1.0	2*s*(F)	−37.7068	↑
$4A_{1g}$	1.0	2*s*(F)	−37.5327	↓
$5A_{1g}$	1.0	3*s*(S)-2*p*(F)^{B}	−23.3760	↑
$5A_{1g}$	1.0	3*s*(S)-2*p*(F)^{B}	−23.2576	↓
$6A_{1g}$	0.0	3*s*(S)-2*p*(F)^{A}	−13.5173	↑
$6A_{1g}$	0.0	3*s*(S)-2*p*(F)^{A}	−13.3554	↓
$7A_{1g}$	0.0		−0.7252	↑
$7A_{1g}$	0.0		−0.6313	↓
$1T_{2g}$	3.0	2*p*(F)	−14.0003	↑
$1T_{2g}$	3.0	2*p*(F)	−13.8139	↓
$2T_{2g}$	0.0	3*d*(S)	−1.4953	↑
$2T_{2g}$	0.0	3*d*(S)	−1.3157	↓
$2E_{g}$	2.0	3*s*(F)	−33.6904	↑
$2E_{g}$	2.0	3*s*(F)	−33.4959	↓
$3E_{g}$	2.0	2*p*(F)	−15.8262	↑
$3E_{g}$	2.0	2*p*(F)	−15.6261	↓
$3T_{1u}$	3.0	3*s*(F)	−34.7694	↑
$3T_{1u}$	3.0	2*s*(F)	−34.5762	↓
$4T_{1u}$	3.0	3*p*(S)-2*p*(F)^{B}	−20.5936	↑
$4T_{1u}$	3.0	3*p*(S)-2*p*(F)^{B}	−20.3650	↓
$5T_{1u}$	3.0	2*p*(F)	−14.6982	↑
$5T_{1u}$	3.0	2*p*(F)	−14.5159	↓
$6T_{1u}$	1.0	3*p*(S)-2*p*(F)^{A}	−3.7416	↑
$6T_{1u}$	0.0	3*p*(S)-2*p*(F)^{A}	−3.5239	↓

[a] The core levels have been left out but their symmetries were considered when numbering the valence levels. The core states are S 1*s* ($1a_{1g}$), F 1*s* ($2a_{1g}$, $1t_{1u}$, $1e_{g}$), S 2*s* ($3a_{1g}$), and S 2*p* ($2t_{1u}$).

[b] The characters here are based on the MT charge decomposition on the atomic spheres while the labels A and B correspond to bonding and antibonding levels, respectively. Blanks are left when the atomic states do not hybridize enough or at all.

transition (there are 0.21 units of charge on the S muffin-tin sphere for the $5a_{1g}$ state compared to 0.05 for the $6a_{1g}$). The corresponding multielectron final-state configuration is $1s^{-1}5a_{1g}^{-1}6a_{1g}6t_{1u}$ and lies approximately 10 eV above the $1s^{-1}6t_{1u}$ transition. We identify this transition with feature *C* lying approximately 8 eV above *B*.

Concomitant with these two multielectron main lines, there are other possible double-electron transitions corresponding to the passive electron transitions $4a_{1g} \rightarrow 6a_{1g}$ (approximately 24 eV above the main line *B* and identified with the feature *E*) and to the transition $5t_{1u} \rightarrow 6t_{1u}$ (approximately 11 eV above *B* and identified with the transition companion to feature *C*). On the basis of charge overlap these last two features are expected to be weaker than those corresponding to the bonding-antibonding transitions of the passive electrons. The possible photoelectron transitions $1t_{2g} \rightarrow 2t_{2g}$ can be excluded on the basis of the fact that the charge overlap is exactly zero, since the molecular orbital, made up of $2p$ F states, resides completely on the F atoms. We defer to a future publication a more thorough discussion on these transitions together with the one-electron calculation of the S *L*-edge spectra, which would give a more coherent picture of the various photoabsorption spectra of SF_6.

C. MS analysis intermediate and single-scattering regions

We attempt now an analysis of the SF_6 photoabsorption spectrum in the framework of the MS theory. Figure 3(a) shows the measured spectrum relative to the S $1s$ ionization threshold energy of 2490 eV in a range up to 350 eV in photoelectron kinetic energy, not corrected for self-absorption. The labels *D*, *E*, *F*, and *G* are the same as those in Fig. 1(a) and have been placed here to maintain our convention. It is important to try to determine properly the various MS regions before carrying out our analysis. In Fig. 3(b) we plot the absorption cross section calculated using the real HL potential with (dotted line) and without (solid line) an outer sphere. The inset shows the spectral radius $\rho(TG)$ of both computations over the same energy range. We see that the presence of an outer-sphere potential has only a slight influence on the cross section which is more pronounced at lower energies where $\rho(TG)$ is larger. The dashed line shows the S atomic absorption, calculated for the muffin-tin atom.

Figure 3(c) shows the same calculation obtained by using the full complex HL potential [see Eq. (3.18)] for the case without an outer-sphere potential and the inset shows the corresponding spectral radius. The calculation with the outer sphere is indistinguishable from this. As expected, the introduction of photoelectron damping in the final state improves the rate of convergence of the MS series and makes absorption features smoother. A convolution of the spectra in Fig. 3(b) with a Lorentzian broadening function using the damping parameter obtained from the inverse of the core hole and photoelectron lifetimes in the final state as given by the imaginary part of the HL potential provides essentially the same result (see Ref. 32) as shown in Fig. 3(c). The advantage of computing with a complex potential lies in the possibility

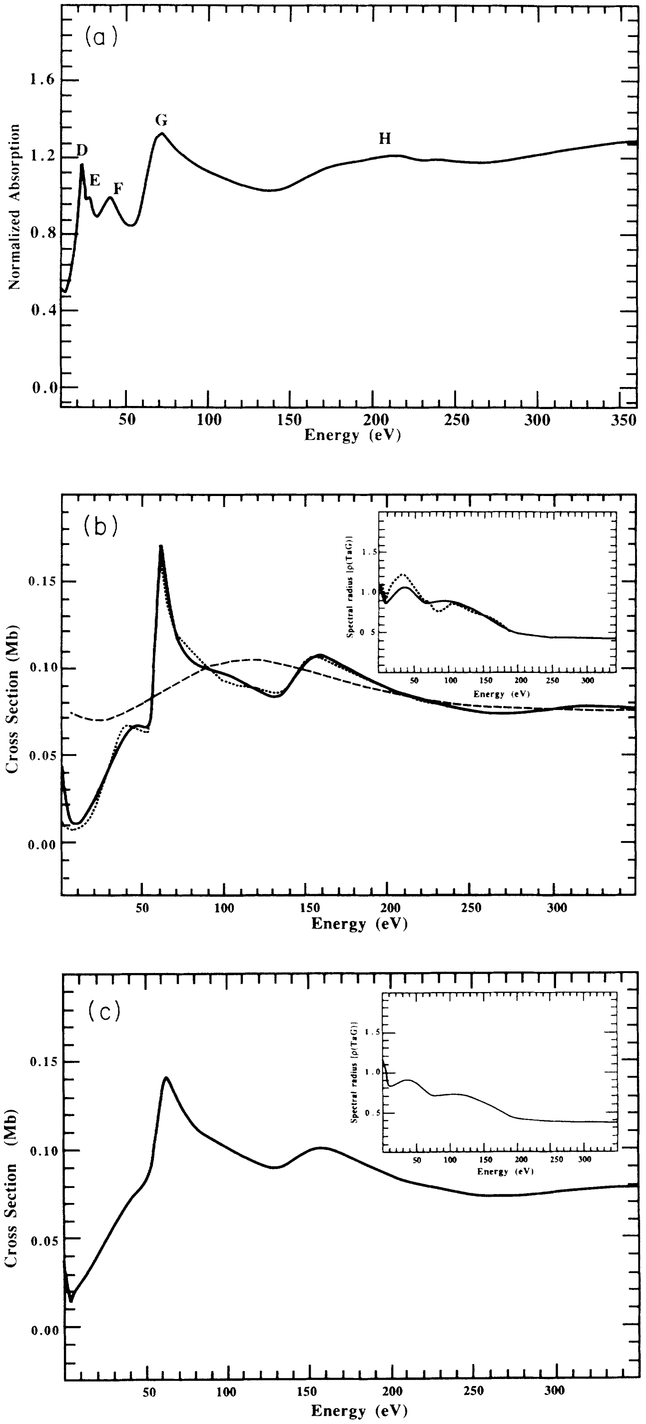

FIG. 3. SF_6 FMS, IMS, and SS regions: (a) The measured spectrum covering the FMS, IMS, and SS regions. (b) Absorption cross sections for calculations utilizing the real HL exchange potential with (dotted line) and without (solid line) an outer sphere. The calculated atomic absorption for the case with no outer sphere has also been plotted (dashed line). (b inset) $\rho(TG)$ for these calculations with (dotted line) and without (solid line) an outer sphere. (c) Absorption cross section computed via the complex HL exchange-correlation potential for the case of no outer sphere. (c inset) $\rho(TG)$ for the corresponding calculation. The case with outer sphere is indistinguishable from this.

of a direct determination of the convergence rate of the MS series in the presence of photoelectron damping. This fact is of the utmost importance in the determination of the number of MS paths present in a photoabsorption spectrum.

Following the systematic division laid down in Sec. II, we can divide the calculated absorption spectrum into three energy regions: a FMS region $[\rho(TG)\geq 0.75]$ covering the energy range up to 70 eV photoelectron energy, an IMS region $[0.75\geq\rho(TG)\geq 0.50]$ covering the range $160\geq E\geq 70$, and a SS region covering the range $E\geq 160$ $[0.50\geq\rho(TG)]$. We note however that due to the strong scattering power of the S and F atoms that the region for which $\rho(TG)\geq 0.70$ extends up to 130 eV of photoelectron energy. This is equivalent to extending the FMS region as far as 130 eV. The important point is that $\rho(TG)$ is approximately 0.75 in the vicinity of the resonance labeled G. This allows us to implement an analysis in terms of MS paths.

Figure 4(a) shows a comparison between the experimental signal $\chi_{\text{exp}}(k)$ derived in the standard way[36] and the theoretical SS signal $\chi_2(k)$ calculated according to Eq. (3.18b) and multiplied by a Debye-Waller function $\exp(-2\sigma^2k^2)$, with σ^2 given by the experimental value listed in Table I.[50] The experimental resolution and core-hole lifetime broadening were found to have a negligible effect on the signal amplitude. The actual comparison in Fig. 4 is between $k\chi_{\text{exp}}(k)$ and $k\chi_2(k)$ in order to blow up the high-k region. Note that there is no adjustment of the photoelectron reference level, which has been taken to be the physical ionization threshold in both spectra. This alignment is the natural one and cannot be otherwise, since in our theoretical treatment the reference level is different in different regions of space and depends on energy. In fact in the interstitial region the photoelectron wave vector $\kappa=(E-\langle V_{II}\rangle)^{1/2}$ is energy dependent through the exchange and correlation part of the interstitial potential $\langle V_{II}\rangle$. In the outer sphere instead we have $k=E^{1/2}$, E being the photoelectron kinetic energy.

From Fig. 4(a) we see that the SS signal models rather accurately the experimental data for $k\geq 6$ Å^{-1} ($E\geq 130$ eV) which is the region in which we expect MS contributions to be negligible. Note that there are no free parameters in the theory except the choice of the atomic radii used in the muffin-tin approximation of the potential which were chosen according to the prescription of Norman,[51] and the α values taken from Schwarz[52] for SCF-SW-$X\alpha$ calculations. We have found that, in the single-scattering region, reducing the 10% overlap of MT radii (keeping the Norman ratio fixed) does not change our results.

A mismatch in phase is observed at lower-k values where the spectral radius is greater than 0.7, pointing to the fact that a SS signal is insufficient to reproduce the experimental curve. Figure 4(b) shows the difference between the measured spectrum and the calculated SS signal (solid line) plotted against a calculated MS signal which includes contributions from all double-, triple-, and quadruple-scattering paths (dotted line, $\chi_3+\chi_4+\chi_5$). The inset displays the separate MS contributions. Among these MS contributions the signals corresponding to collinear paths are the dominant ones since they are enhanced by the focusing effect and because the orthogonality rule approximately depresses all of the other noncollinear paths where the first and last vectors joining the central S atom and the F ligand are orthogonal.[12(a)] The dashed line in Fig. 4(b) represents the contributions of the triple-scattering paths of the type: S-F1-S-F1-S, S-F1-S-F1′-S, and S-F1-S-F2-S where F1 and F1′ are *trans* and F1 and F2 are *cis*.[53] It is seen that there is reasonable amplitude agreement with the experimental residual signal at least for the first three oscillations. At higher-k values the noise level does not allow us to extend the comparison further. This approximate agreement indicates that other MS paths, certainly present in the spectrum due to the large value of $\rho(TG)$ (approximately 0.80) roughly cancel one another. In our experience, this

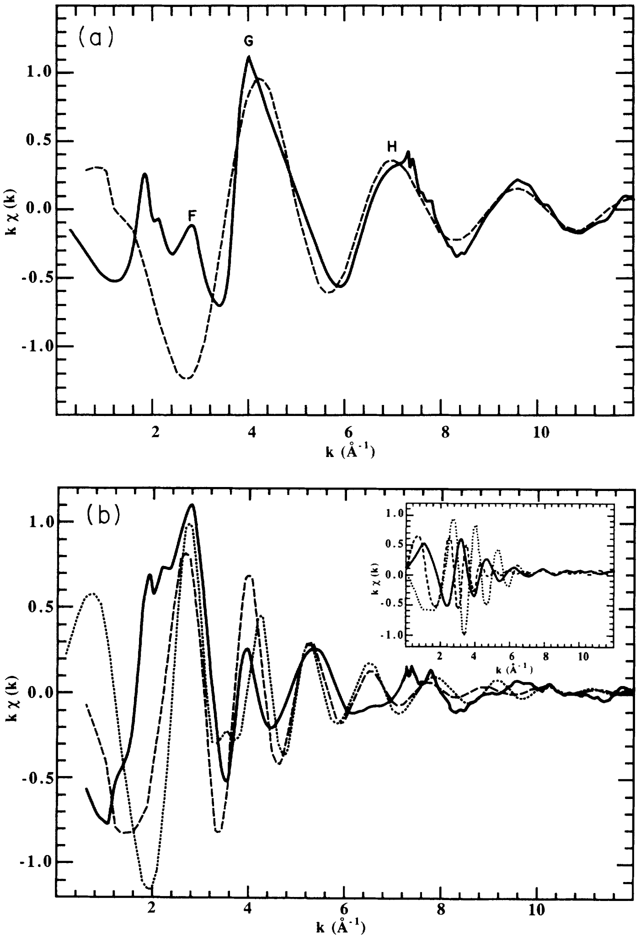

FIG. 4. SF$_6$ measured EXAFS and calculated single-scattering spectra: (a) The solid line is the measured EXAFS spectrum weighted by k while the dashed line is the computed single-scattering spectrum also weighted by k. (b) The difference between the measured EXAFS spectrum and calculated single-scattering spectrum (solid line), the sum of the contributions from all double, triple, and quadruple MS paths (dotted line) and the dominant triple-scattering signals (dashed line) of the type S-F1-S-F1-S, S-F1-S-F1′-S, S-F1-S-F2-S, where F1 and F1′ are *trans* while F1 and F2 are *cis*. [(b) inset] individual double (solid line), triple (dotted line), and quadruple (dashed line) MS signals.

is generally the rule in high-symmetry coordination geometries. However in order to reproduce the exact shape of the *F* and *G* resonances the contribution of all these paths would be essential. This situation reinforces the claim that feature *G* is a shape resonance, since it requires many MS paths to reproduce its shape. Due to the fortunate case that the resonance falls in a high-energy regime with spectral radius approximately 0.75, we were able to do a meaningful analysis in terms of MS paths (since the series is convergent) and extract the dominant carrier waves among the various signals.

D. Summary

In summary, on the basis of an effective one-electron picture we have been able to assign features *B*, *F*, and *G* to dipole-allowed final-state channels of t_{1u} symmetry as bound state (*B*) or continuum resonances (*F* and *G*). An eigenphase shift analysis has shown the antiresonance character of feature *F*, which is very sensitive to the details of the molecular potential, whereas *G* has been interpreted as a "delayed" shape resonance of centrifugal barrier type. No features *D* and *E* appear in this description. Unless one wants to resort to improbable dipole-forbidden transitions, the only explanation left relies on their multielectron character which seems to be confirmed by a study of the energetics of the double-electron transition. We therefore agree with the interpretation proposed by Ferrett *et al.*[38] both on the basis of their analysis of photoelectron spectra in SF_6 and preliminary MS calculations. We defer to future work, incorporating both vibrational and multielectron effects, the assignment of features *A* and *C*. As a conclusion, we share the conviction, put forward by Ferrett *et al.*[54] in a second study of S 2*p* photoionization, that "SF_6 is most likely a very special case which provides us with a testing ground for investigating unusually strong many-electron interactions in molecules." Being equipped with a suitable theoretical framework to describe this type of situation[28,49] we will take up this challenge in future investigations.

VI. APPLICATION OF GENERAL METHODS TO $GeCl_4$

As an example of the utility of the method developed here we compare the results of our own computations with the experiments and computations of the MS spectrum of $GeCl_4$ carried out by Bouldin *et al.*[55] In order to fully understand the range of the MS signals the Ge *K*-edge spectra of the gases GeH_4, GeH_3Cl, and $GeCl_4$ were measured. The measurements were done in the transmission mode using ion chamber detectors and a Si(111) monochromator. With this experimental configuration an experimental resolution of 3.5 eV was reported. One should note that the measured amplitudes are about a factor of 2 higher than those reported in Ref. 10(a), which were taken from Kincaid's thesis.[56] The same problem is found in Br_2 and will be mentioned in Sec. VII.

To experimentally determine the range of the MS signal, the data were first normalized and then a subtraction procedure was implemented. It was assumed that the GeH_4 spectrum could be used as a model for the Ge *K*-edge atomic absorption while that of GeH_3Cl would yield $\frac{1}{4}$ the $GeCl_4$ single-scattering spectrum (plus atomic absorption). Hence the linear combination $\Delta\chi = \chi_{GeCl_4} - 4\chi_{GeH_3Cl} + 3\chi_{GeH_4}$ was taken to represent the MS signal ($n > 2$) in the $GeCl_4$ spectrum. The following conclusions were drawn from the analysis.

(1) The SS signal dominates the MS signal even at low energies.

(2) Only within 15 eV of the edge is the MS signal comparable in amplitude to the SS signal.

(3) The ratio of the MS to SS amplitudes decays to less than 6% beyond 40 eV of the edge.

In order to "obtain a good idea of the current state of theoretical calculations compared with experiment" multiple-scattering computations were also carried out by Bouldin *et al.*[55] Here as in the case of the experimental measurements we outline the basic content of their calculations. First of all a non-SCF molecular potential was constructed by the overlapping atomic potentials generated from SCF Herman-Skillman[57] charge densities for neutral Ge and Cl atoms. From the brief outline given it is not clear what potential was used for the final state. But it may have been the standard $Z+1$ potential used in non-SCF computations.[58] The formulation of Durham *et al.*[59] was used to compute the total multiple-scattering signal. It should be noted that this formulation allows for the damping of the photoelectron via the inclusion of the sum of the core-hole and excited state lifetimes as a constant imaginary part of the potential but its use was not discussed. In the computations the atomic radii for Ge and Cl were defined to be 2.5 and 2.1 atomic units, respectively. The single-scattering spectrum was calculated using the formalism of Müller and Schaich.[60] To obtain the MS signal the computed SS signal was subtracted from the computed total MS signal and the following observations were made.

(1) Beyond 40 eV of the edge the MS signal is negligible.

(2) The ratio of the MS signal to the SS signal is 15% above 40 eV.

In summarizing the following statements on which we will focus were made.

(1) "Because of the path lengths involved, MS can always be neglected for EXAFS studies of the first shell."

(2) When $k \gtrsim 3$ Å^{-1} (40 eV) MS signals ($n > 2$) may be neglected.

(3) "Theoretical simulations are not yet quantitatively accurate. They tend to overestimate the importance of multiple scattering relative to single scattering."

In order to subject our *ab initio* method to another system in which extensive data were available we decided to attempt to see how close we could get to the results of the $GeCl_4$ experiments. Our computations were identical to those carried out for SF_6. Spin-polarized ground-state and excited-state SCF-SW-$X\alpha$ potentials were constructed for $GeCl_4$. (See Table I for computational information.) The final-state potential was one with the configuration $1s^{-1}t_2$, which produced a t_2 level with the highest charge on the Ge atomic sphere and hence was assumed to correspond to the experimental white line. The term energy $\Delta E = E_{1s\rightarrow\infty} - E_{1s\rightarrow t2} = 6.3$ eV was used to place the onset of the continuum at 6.3 eV above the experimental white line. In order to compare our computational results with those of Bouldin *et al.*[55] we note that the experimental white line is set at 17.3 eV.[50] Hence the onset of the continuum must be at 23.6 eV. In this way we are able to place our energy scale relative to theirs.

We display the total fine-structure signal (solid line), the SS (dotted line) signal, and the sum of the first three MS signals (dashed line, $n = 3$, 4, and 5) in Fig. 5(a) (above 50 eV this latter is indistinguishable from the difference of the first two curves. As an inset we also present the spectral radius. All of the computations were obtained via the EC-MS-CHL using no outer-sphere potential. Notice that above 50 eV (despite the fact that the spectral radius is close to 0.5) the SS and total fine-structure signal are very close in amplitude and phase, pointing to the fact that the residual MS signal is very weak (less than 5% of the SS signal) in agreement with the experimental finding of Bouldin *et al.*[55] This fact can be understood by looking at the individual MS signals [Fig. 5(b)] corresponding to double-scattering (solid line), triple-scattering (dotted line), and quadruple-scattering (dashed line) paths. It is clear that although the signals have appreciable amplitude individually [about 15–30% of the SS signal, in keeping with the value of $\rho(TG) \approx 0.5$], their sum is affected by a massive cancellation.

In order to assess the amplitude of the SS signal we have included an experimental Debye-Waller factor[61] (see Table I) and total resolution width of 4 eV (via Gaussian convolution) composed of the core-hole lifetime [1.9 eV (Ref. 46)] and the experimental resolution [3.5 eV (Ref. 55)]. In Fig. 5(c) we compare our single-scattering spectrum directly with the experimental spectrum ($GeCl_4$) of Bouldin *et al.*[55] First of all we see that there is no problem with the amplitude of the computed spectrum and hence the last conclusion of Bouldin *et al.*[55] is not valid for our model. We note however that there is a slight mismatch of the phases which we think may be due to the exchange-correlational potential used or the MT parameters used. In fact, although we have tried to adopt physical criteria to minimize the effect of the arbitrariness in the selection of these parameters it is clear that some dependence still exists. Slightly changing the Norman ratio of the MT radii improves the agreement with experimental data. Also, one should consider the possibility of an error of 2–3 eV in the relative positioning of the theoretical and experimental energy scales due to either an imprecise estimate of the term energy or to our inability to accurately position the experimental EXAFS spectrum.) Parts 1 and 2 of the conclusions by Bouldin *et al.*[55] as a unit are equally invalid because as seen in Fig. 5(b) the individual MS signals are not negligible in the low-energy region but it is their sum that, in this case, is small. We draw the following conclusions from our study.

(1) The absence of a large MS signal in experimental data does not indicate the absence of individual MS signals. It might well happen that a cancellation, resulting from the particular geometry and atomic phase shifts involved, will not occur in a different geometrical arrangement and/or with different type of ligands. It is therefore possible to reconcile the apparently contradicting

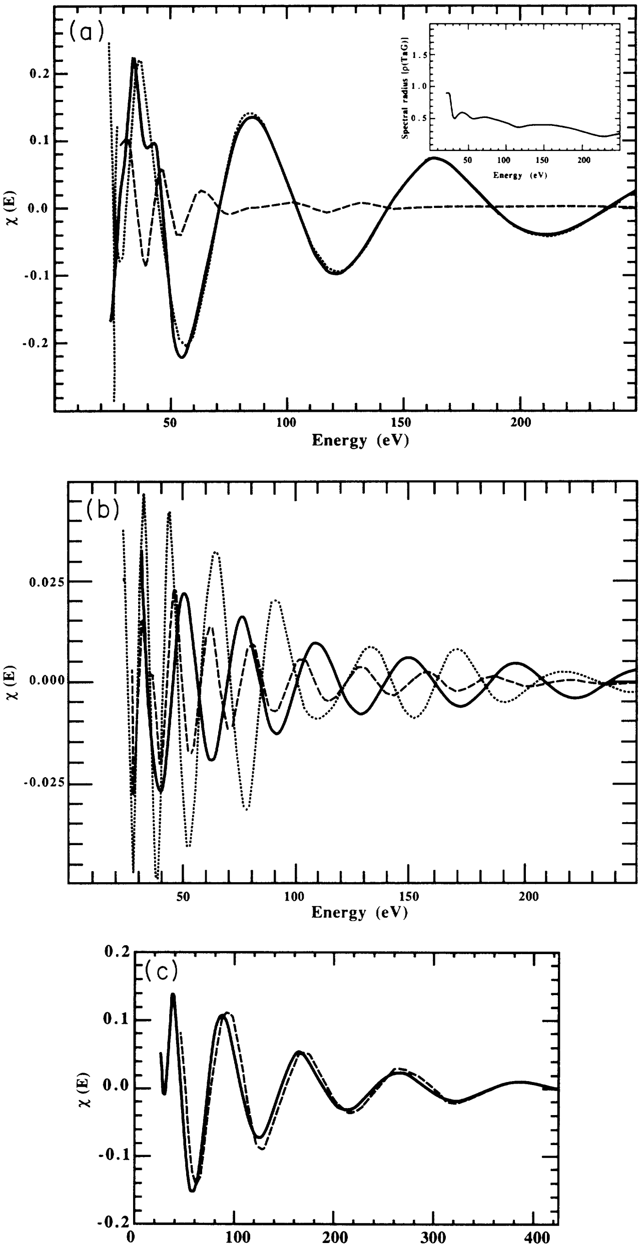

FIG. 5. (a) Total fine-structure signal (solid line), the SS signal (dotted line), and the sum of all MS paths of order $n = 3,4,5$ (dashed) for $GeCl_4$ computed via the EC-MS-CHL method. In practice this latter curve coincides with the difference between the first two curves. (a inset) Spectral radius $\rho(TG)$. (b) Individual MS signals corresponding to double scattering (solid line), triple scattering (dotted line), and quadruple scattering (dashed line). (c) Comparison of the computed single-scattering spectrum (solid line) with the experimental spectrum (dashed line).

findings in $GeCl_4$ (see Ref. 55) and MnO_4^- [see Ref. 12(a)] concerning the amount of MS signal present in the respective absorption spectra.

(2) It is dangerous to draw general conclusions from single experimental cases since it is quite possible that the case chosen is not representative. The comparison with the case of SF_6, discussed in the preceding section, is illuminating in this respect. Here very strong MS effects in the form of a shape resonance occur at about 70 eV above the edge and to a lesser extent (as deviation from single scattering) persist up to 150 eV ($k=6$ Å^{-1}).

VII. APPLICATION OF GENERAL METHODS TO Br_2

As a final application of our formalism we compare our computation of the SS spectra of Br_2 with the result of Chou *et al.*[7] In order to develop a prescription for the computation of SS spectra by *ab initio* methods, Chou *et al.*[7] undertook, as mentioned above, a rather extensive study of the effects of different exchange-correlation potentials and models of relaxation (using time-dependent perturbation theory to first order).

As experimental data, use was made of the measurements of Stern *et al.*[62] which are an improvement over the measurements of Kincaid and Eisenberger.[63] It was found that due to the reaction of the Br_2 gas with the Kapton x-ray windows, the original experimental data had amplitudes which were too low by a factor of 3. This can be seen by comparing Fig. 9 of Ref. 7 with Fig. 3 of Ref. 63.

With regard to the construction of the initial-state and final-state potentials the approach of Chou *et al.*[7] was almost identical to ours. By using the Norman method[51] and setting the atomic radii such that $0.88Z$ (Z = atomic number) units of charge are enclosed in each atomic sphere, they set the radii of the Br and outer sphere to be 2.74 and 4.89 atomic units, respectively. Given a bond distance of 4.31 atomic units this results in 27% overlap of the atomic spheres. They found that these radii yield approximate compliance with the virial theorem as well as agreement of calculated ionization energies and transition energies with experimental values. Using the SCF-SW-$X\alpha$ approach, a ground-state potential was obtained. For the excited-state potential the completely ionized configuration was chosen. For the determination of the photoelectron wave vector k the term energy $\Delta E = E_{1s\rightarrow\infty} - E_{1s\rightarrow 4\sigma} = 8$ eV was used to determine how high above the white line the continuum onset began. $E_0 = E(k=0)$ was then determined via the final-state MT constant interstitial potential (-10 eV) to be 2 eV below this $1s\rightarrow 4\sigma$ white line. A full spherical wave expression was used to compute the SS signal. In addition, they included a calculated Debye-Waller factor.

In summarizing their conclusions on the appropriate prescriptions needed to obtain agreement with experiments the following statements were made.

(1) A dynamic exchange-correlation potential is necessary.

(2) The Dirac-Hara exchange gives better phase agreement than the HL exchange-correlation potential.

(3) Intrinsic losses must be included in order to get good amplitude agreement with experiments.

In a way similar to our analysis of the spectra of SF_6 and $GeCl_4$ we carried out a computation of the single- and multiple-scattering signals of Br_2. Spin-polarized ground-state and excited $1s\rightarrow 4\sigma$ state configurations were obtained by using nonoverlapping spheres (the radii are given in Table I) via the SCF-SW-$X\alpha$ scheme. The final σ valence level again was chosen such that it placed the maximum charge on the Br sphere when self-consistency was reached. The transition was assumed to correspond to the experimental white line. The term energy $\Delta E = E_{1s\rightarrow\infty} - E_{1s\rightarrow 4\sigma} = 8.3$ eV was found to be quite close in magnitude to the spin-up interstitial potential value of -8.33 eV. Using this term energy the k scale in the experimental spectrum was determined just as was done for SF_6.

We follow again the same approach used for the other molecules and use the SCF-MS-CHL method with no outer-sphere potential. In Fig. 6(a) we display the total fine-structure signal (solid line), the single-scattering signal (dotted line), and total triple-scattering signal (dashed line) since there is no double-scattering path in a diatomic molecule. Note that the net nonpolarized signal is a combination of the signals corresponding to the $\sigma(z)$ and

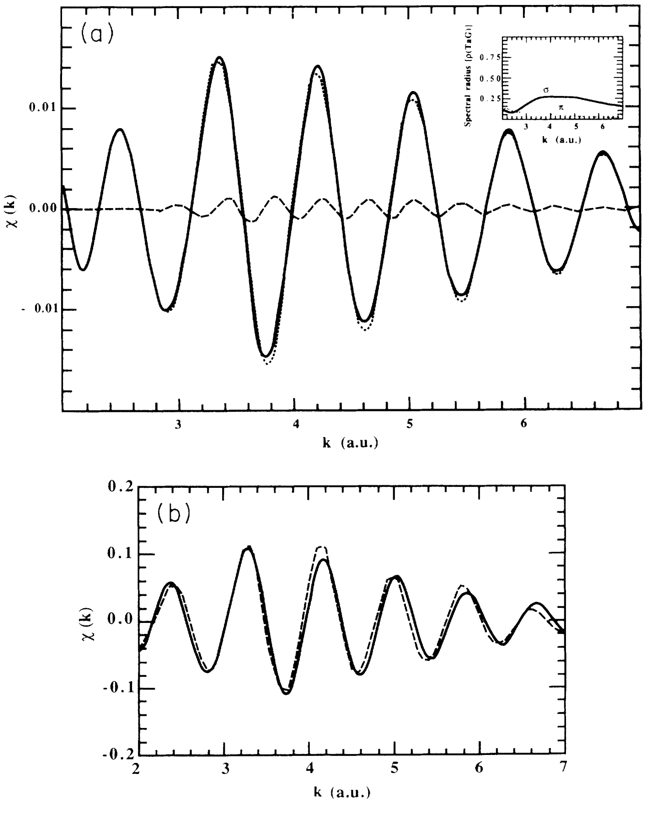

FIG. 6. (a) Total fine-structure signal (solid line), SS signal (dotted line), and triple-scattering signal (dashed line) for Br_2 computed via the SCF-MS-CHL method. (a inset). The spectral radius $\rho(TG)$ for the σ and π polarization spectra. (b) Comparison of the computed single-scattering spectrum (solid line) with the experimental spectrum (dashed line).

$\pi(x,y)$ irreducible representations of the $C_{\infty v}$ point group combined via the relation

$$\chi_n = [\chi_n^{\sigma} + 2\chi_n^{\pi}]/3 \ .$$

We remark that the triple-scattering signal is small below $k=3$ (a_0^{-1}) increases near this value and then decreases above $k=6$ (a_0^{-1}). (Atomic units are used here to facilitate direct comparison with the results of Ref. 7.) This behavior can be understood by looking at the spectral radius $\rho(TG)$ shown in the inset of Fig. 6(a) and is connected to the value taken by $\sin(\delta_l)$ for the relevant phase shifts in this k region.

In order to further compare our scheme for the computation of χ_2 with that of Chou *et al.*[7] we have taken the single-scattering spectrum and have included in a standard way a Debye-Waller factor[7] (see Table I) together with the amplitude reduction effects due to the core-hole lifetime [2.7 eV (Ref. 46)] and experimental resolution [2.7 eV (Ref. 63)] giving a total width of 3.8 eV. In Fig. 6(b) we compare this calculated single-scattering signal with the experimental spectrum of Ref. 7. As in the case of the other gases there is no problem with amplitude agreement. However, like $GeCl_4$ and unlike SF_6, there is some slight mismatch in phase for which the same considerations as for $GeCl_4$ apply.

Our conclusion is the same as that in Ref. 7 for what concerns point 1. (With regards to point 2, we find that the use of a Dirac-Hara exchange-correlation potential does not seem necessary. Here too further investigations are needed.) We find also that the inclusion of intrinsic losses is not necessary to get amplitude agreement with the experiments. This finding seems to be in favor of an adiabatic turn-on model for intrinsic losses,[64] which tends to give a smaller phasor summation correction (amplitude reduction factor of the order of 0.9) compared to the sudden model (reduction factor of about 0.8).[7] Due to the fact that we have used a computed value for the DW factor (the same as in Ref. 7), we cannot draw any definite conclusion on this problem. Further applications of the theory are needed before a positive statement can be made. We feel however that the amplitude agreement found in the three molecules studied is indicative of the fact that the intrinsic loss corrections are less important than previously thought, at least for what concerns the first coordination shell. We also have indications that this is true for further distant shells.[32]

VIII. CONCLUSIONS

In this paper we have presented a general MS scheme for the calculation and the interpretation of inner-shell x-ray-absorption fine structure for clusters of atoms in condensed matter with application to SF_6 and $GeCl_4$ and Br_2. We have addressed the problem of the equivalence between two traditional approaches: the scattering approach of Dehmer and Dill[2] and the density of states (or MS) approach of Lee and Pendry.[10(a)] By working in T-matrix normalization we have explicitly shown that the former method reduce to the latter in the case of a MT potential with outer sphere, this equivalence holding also for general potentials, as shown in Ref. 4(a). This way it becomes possible to reinterpret concepts such as shape resonances in terms of diffractive interference processes due to many MS paths. Consequently, the difference between a diffractive maximum and a shape resonance is elucidated as discussed in Sec. V A for the case of the SF_6 molecule. The equivalence also highlights the substantial continuity between the two energy regimes in which resonances and diffractive maxima (extended fine structure) are present as is illustrated in the case of SF_6.

In order to take into account extrinsic losses of the photoelectron in the final state, we have generalized the MS approach to a complex absorption potential of the HL[6,7] type, giving a precise prescription for the derivation of the various MS signals and for their comparison with the experimental fine-structure signals. In the three cases studied, after accounting for DW factor and experimental resolution in the proper way, we find amplitude agreement between the calculated and experimental fine-structure signals. This fact might indicate that the correction for the intrinsic loss processes[7] (phasor summation correction) is negligible. Further applications of the method are necessary to substantiate this. In two molecules ($GeCl_4$ and Br_2) we find some slight phase mismatch between the calculated and the experimental signals which might depend on a variety of factors as discussed in Sec. VI.

The possibility of monitoring the expansion parameter $\rho(T_a G)$ of the MS series provides us with an *a priori* reliable knowledge of the number and type of MS paths present in an absorption fine-structure signal beyond the SS one. The application of the theory to $GeCl_4$ confirms the small amplitude of the MS (sum for $n=3,4,5$) contributions[55] (about 5% of the SS signal) as due to a fortuitous cancellation of the paths of order $n=3,4,5$. The same cancellation is not present in the MnO_4^- anion.[12(a)] This is due to the fact that the scattering power of oxygen fades away with increasing energy more rapidly than for chlorine atoms. The consequence of this is a depression of the paths with $n=4,5$ and the inhibition of the destructive interference with the double-scattering paths.

In our experience, there is no general "rule of thumb" to estimate the contribution of MS paths. We have found that the best way to extract these signals is via a fitting-subtraction procedure that fits the dominant sinusoidal contributions and subtracts them from the experimental signal in such a way that the residual signal can be readily analyzed. We have applied this procedure with success to the analysis of *a*-Si in order to bring out effects connected with three-atom correlations.[65]

In conclusion, although more investigation is needed to assess the reliability of the theory, we feel rather confident that it can be applied with success to the analysis of the x-ray-absorption fine-structure data, especially if supplemented with non-MT corrections (which we plan to do in a near future) and a sound final-state effective optical potential. This last aspect of the theory needs further investigation. However, the HL exchange-correlation potential seems to constitute a good starting point for photoelectron energies more than about 30 eV above the ionization threshold.

ACKNOWLEDGMENTS

We are indebted to Dr. B. Hedman (Stanford Synchrotron Radiation Laboratory (SSRL), Stanford University, Stanford, California) for much assistance with our experiments and for reading the drafts of this paper. The authors would like to thank Professor J. J. Rehr (Physics Department, University of Washington, Seattle, Washington) for providing the experimental spectra of Br_2 and $GeCl_4$. This research was supported by National Science Foundation Grant No. CHE 88-17702. The experiments on SF_6 were carried out at SSRL which is supported by the Department of Energy's Office of Basic Energy Science and the NIH's Division of Research Resources, Biomedical Research Technology Program.

---

[1] K. H. Johnson, Adv. Quantum Chem. **7**, 143 (1973).

[2] D. Dill and J. L. Dehmer, J. Chem. Phys. **61**, 692 (1974).

[3] J. A. Tossel and J. W. Davenport, J. Chem. Phys. **80**, 813 (1984) and references therein.

[4] (a) C. R. Natoli, M. Benfatto, and S. Doniach, Phys. Rev. A **34**, 4682 (1986); (b) R. Zeller, J. Phys. C **20**, 2347 (1987); (c) J. Molenaar, *ibid.* **21**, 1455 (1988). (a) and (b) discuss the generalized MS theory in angular momentum representation while (c) gives a representation-independent discussion.

[5] D. L. Foulis, R. F. Pettifer, C. R. Natoli, and M. Benfatto, Phys. Rev. A **41**, 6922 (1990); D. L. Foulis, Ph.D. thesis, University of Warwick, 1988; D. L. Foulis, R. F. Pettifer, and C. R. Natoli, J. Phys. (Paris) C **8**, 597 (1986).

[6] (a) L. Hedin and S. Lundqvist, Solid State Phys. **23**, 1 (1969); J. Phys. (Paris) C **3**, 73 (1972); J. Phys. C **4**, 2347 (1971); **4**, 2064 (1971); (b) J. C. Inkson, *Many-Body Theory of Solids: An Introduction* (Plenum, New York, 1986); (c) A. L. Fetter and J. D. Walecka, *Quantum Theory of Many-Particle Systems* (McGraw-Hill, New York, 1971); (d) G. D. Mahan, *Many Particle Physics* (Plenum, New York, 1981). (b) gives an intuitive development of many-body theory including a discussion of the work given in (a) while (c) and (d) give more formal developments of many-body theory.

[7] S.-H. Chou, J. J. Rehr, E. A. Stern, and E. R. Davidson, Phys. Rev. B **35**, 2604 (1987).

[8] (a) F. W. Kutzler, C. R. Natoli, D. K. Misemer, S. Doniach, and K. O. Hodgson, J. Chem. Phys. **73**, 3274 (1980); (b) C. R. Natoli, D. K. Misemer, S. Doniach, and F. W. Kutzler, Phys. Rev. A **22**, 1104 (1980).

[9] (a) S. Doniach, M. A. Berding, T. Smith, and K. O. Hodgson, in *EXAFS and Near Edge Structure III,* edited by K. O. Hodgson, B. Hedman, and J. E. Penner-Hahn (Springer-Verlag, Berlin, 1984), p. 3; (b) M. A. Berding, Ph.D. thesis, Stanford University, 1985.

[10] (a) P. A. Lee and J. B. Pendry, Phys. Rev. B **11**, 2795 (1975); (b) C. R. Natoli and M. Benfatto, J. Phys. (Paris) C **8**, 11 (1986); (c) D. D. Vvedensky, D. K. Saldin, and J. B. Pendry, Comput. Phys. Commun. **40**, 421 (1986).

[11] P. A. Lee and G. Beni, Phys. Rev. B **15**, 2862 (1977).

[12] (a) M. Benfatto, C. R. Natoli, A. Bianconi, J. Garcia, A. Marcelli, M. Fanfoni, and I. Davoli, Phys. Rev. B **34**, 5774 (1986); (b) W. A. Schaich, *ibid.* **29**, 6513 (1984).

[13] J. J. Rehr, R. C. Albers, C. R. Natoli, and E. A. Stern, Phys. Rev. B **34**, 4350 (1986).

[14] G. Breit and H. A. Bethe, Phys. Rev. **93**, 888 (1954).

[15] J. R. Taylor, *Scattering Theory* (Wiley, New York, 1972); R. H. Landau, *Quantum Mechanics II: A Second Course in Quantum Theory* (Wiley, New York, 1990); J. S. Faulkner, J. Phys. C **10**, 4611 (1977).

[16] R. S. Mulliken, J. Am. Chem. Soc. **86**, 3183 (1964); U. Fano, Comments At. Mol. Phys. **3**, 75 (1972).

[17] (a) D. Dill and J. L. Dehmer, Phys. Rev. Lett. **35**, 213 (1975); (b) J. L. Dehmer and D. Dill, J. Chem. Phys. **65**, 5327 (1976).

[18] J. R. Swanson, D. Dill, and J. L. Dehmer, J. Chem. Phys. **75**, 619 (1981).

[19] C. R. Natoli, in *EXAFS and Near Edge Structure,* edited by A. Bianconi, L. Incoccia, and S. Stipcich (Springer-Verlag, Berlin, 1983), p. 43.

[20] A. Bianconi, M. Dell'Ariccia, A. Gargano and C. R. Natoli, in *EXAFS and Near Edge Structure* (Ref. 19), p. 57.

[21] C. R. Natoli, in *EXAFS and Near Edge Structure III* [Ref. 9(a)], p. 38.

[22] F. Sette, J. Stöhr, and A. P. Hitchcock, J. Chem. Phys. **81**, 4906 (1984).

[23] (a) A. Bianconi, E. Fritsch, G. Calas, and J. Petiau, Phys. Rev. B **32**, 4292 (1985); (b) F. W. Lytle, R. B. Greegor, and A. J. Panson, *ibid.* **37**, 1550 (1988).

[24] A. Bianconi, A. Di Cicco, N. V. Pavel, M. Benfatto, A. Marcelli, C. R. Natoli, P. Pianetta, and J. Woicik, Phys. Rev. B **36**, 6462 (1987).

[25] M. Benfatto, C. R. Natoli, J. Garcia, and A. Bianconi, J. Phys. (Paris) C **8**, 25 (1986).

[26] (a) P. A. Lee, P. H. Citrin, P. H. Eisenberger, B. Kincaid, Rev. Mod. Phys. **53**, 769 (1981); (b) S. J. Gurman, J. Phys. C **21**, 3699 (1988).

[27] A. Filipponi, A. Di Cicco, T. A. Tyson, and C. R. Natoli, Solid State Commun. **78**, 265 (1991); A. Filipponi, A. Di Cicco, R. Zanoni, M. Bellatriccia, V. Sessa, C. Dossi, and R. Psaro, Chem. Phys. Lett. **184**, 485 (1991); A. Di Cicco, S. Stizza, A. Filipponi, F. Boscherini, and S. Mobilio, J. Phys. B **25**, 2309 (1992).

[28] C. R. Natoli, M. Benfatto, C. Brouder, M. Ruiz-Lopez, and D. L. Foulis, Phys. Rev. B **42**, 1944 (1990).

[29] J. E. Müller and J. W. Wilkins, Phys. Rev. B **29**, 4331 (1984); J. E. Müller, O. Jespen, and J. W. Wilkins, Solid State Commun. **42**, 365 (1982).

[30] A. Filipponi, E. Bernieri, and S. Mobilio, Phys. Rev. B **38**, 3298 (1988).

[31] D. R. Penn, Phys. Rev. B **35**, 482 (1987).

[32] P. Sainctavit, J. Petiau, M. Benfatto, and C. R. Natoli (unpublished).

[33] J. S. Faulkner and G. M. Stocks, Phys. Rev. B **21**, 3222 (1980).

[34] E. Stern and S. Heald, Rev. Sci. Instrum. **50**, 1579 (1979).

[35] F. W. Lytle, R. B. Greegor, D. R. Sandstrom, E. C. Marques, J. Wong, C. L. Spiro, G. P. Huffman, and F. E. Huggins, Nucl. Instrum. Methods **226**, 542 (1984).

[36] S. P. Cramer and K. O. Hodgson, in *Progress in Inorganic Chemistry,* edited by S. J. Lippard (Wiley, New York, 1979), Vol. 25, p. 1; T. A. Tyson, A. L. Roe, P. Frank, K. O. Hodgson, and B. Hedman, Phys. Rev. B **39**, 6305 (1989).

[37] R. E. LaVilla and R. D. Deslattes, J. Chem. Phys. **44**, 4399 (1966).

[38] T. A. Ferrett, D. W. Lindle, P. A. Heimann, H. G. Kerkhoff, U. E. Becker, and D. A. Shirley, Phys. Rev. B **34**, 1916 (1986).

[39]F. A. Gianturco, C. Guidotti, and U. Lamanna, J. Chem. Phys. **57**, 840 (1972).

[40](a) T. M. Zimkina and A. S. Vinogradov, J. Phys. (Paris) C **4**, 3 (1971); (b) J. L. Dehmer, J. Chem. Phys. **56**, 4496 (1972).

[41]V. Nefedov, J. Struct. Chem. **11**, 277 (1970).

[42]J. L. Dehmer, D. Dill, and A. C. Parr, in *Photophysics and Photochemistry in the Vacuum Ultraviolet,* edited by S. P. McGlynn, G. L. Findley, and R. H. Huebner (Reidel, Dordrecht, 1985), p. 341.

[43]H. Nakamatsu, T. Mukoyama, and H. Adachi, Chem. Phys. **143**, 221 (1990).

[44]A. P. Hitchcock, M. Pocock, and C. E. Brion, Chem. Phys. Lett. **49**, 125 (1977). For a discussion of the theory of vibronically coupled electronic transitions see G. Fischer, *Vibronic Coupling* (Academic, London, 1984).

[45]R. S. Wallace, Ph.D. thesis, Boston University, 1980.

[46]M. O. Krause and J. H. Oliver, J. Phys. Chem. Ref. Data **8**, 329 (1979); V. O. Kostroun, M. H. Chen, and B. Crasemann, Phys. Rev. A **3**, 533 (1971); J. H. Scofield, Phys. Rev. **179**, 9 (1969).

[47]G. Garcia, A. Bianconi, M. Benfatto, and C. R. Natoli, J. Phys. (Paris) C **8**, 49 (1986).

[48]U. Fano and J. W. Cooper, Rev. Mod. Phys. **40**, 441 (1986).

[49]T. A. Tyson, Ph.D. thesis, Stanford University, 1991.

[50]B. R. Miller and M. Fink, J. Chem. Phys. **75**, 5326 (1981).

[51]J. G. Norman, Jr., Mol. Phys. **31**, 1191 (1976).

[52]K. Schwarz, Phys. Rev. B **5**, 2466 (1972).

[53]T. A. Tyson, M. Benfatto, C. R. Natoli, B. Hedman, and K. O. Hodgson, Physica B **158**, 425 (1989).

[54]T. A. Ferrett, D. W. Lindle, P. A. Heimann, M. N. Piancastelli, P. H. Kobrin, H. G. Kerkhoff, U. Becker, W. D. Brewer, and D. A. Shirley, J. Chem. Phys. **89**, 4726 (1988).

[55]C. E. Bouldin, G. Bunker, D. A. McKeown, R. A. Forman, and J. J. Ritter, Phys. Rev. B **38**, 10 816 (1988).

[56]B. M. Kincaid, Ph.D. thesis, Stanford University, 1975.

[57]F. Herman and S. Skillman, *Atomic Structure Calculations* (Prentice-Hall, Englewood Cliffs, 1963).

[58]P. J. Durham, in *X-Ray Absorption,* edited by D. C. Koningsberger and R. Prins (Wiley, New York, 1988), p. 53.

[59]P. J. Durham, J. B. Pendry, and C. H. Hodges, Comput. Phys. Commun. **25**, 193 (1982).

[60]J. E. Müller and W. L. Schaich, Phys. Rev. B **27**, 6489 (1983).

[61]Y. Marino, Y. Nakamura, and T. Iijima, J. Chem. Phys. **32**, 643 (1960).

[62]E. A. Stern, S. M. Heald, and B. Bunker, Phys. Rev. Lett. **42**, 1372 (1979).

[63]B. M. Kincaid and P. Eisenberger, Phys. Rev. Lett. **34**, 1361 (1975).

[64]T. A. Thomas, Phys. Rev. Lett. **52**, 417 (1984).

[65]A. Filipponi, A. Di Cicco, M. Benfatto, and C. R. Natoli, Europhys. Lett. **13**, 319 (1990); A. Filipponi, F. Evangelisti, M. Benfatto, S. Mobilio, and C. R. Natoli, Phys. Rev. B **40**, 9636 (1989).